ELSEVIER

Journal of Fluids and Structures 22 (2006) 617–645

JOURNAL OF FLUIDS AND STRUCTURES

www.elsevier.com/locate/jfs

A flexible rod in annular leakage flow: Influence of turbulence and equilibrium offset, and analysis of instability mechanisms

M.A. Langthjem[a,*], H. Morita[b], T. Nakamura[c], M. Nakano[a]

[a]*Department of Mechanical Systems Engineering, Yamagata University, 4-3-16 Jonan, Yonezawa-shi, Yamagata 992-8510, Japan*
[b]*Takasago Research and Development Center, Mitsubishi Heavy Industries, Ltd., 2-1-1 Shinhama, Arai-cho, Takasago-shi Hyogo 676-8686 Japan*
[c]*Department of Mechanical Engineering, Osaka Sangyo University, 3-1-1 Nakagaito, Daito-shi, Osaka 574-8530, Japan*

Received 9 August 2004; accepted 22 March 2006

Abstract

The linear stability of a flexible, cylindrical rod subjected to annular leakage flow is studied. The mathematical models developed by Li, Kaneko, and Hayama in 2002 and Fujita and Shintani in 2001 are bridged and extended, to account for a flexible rod with equilibrium offset (eccentricity) in laminar or turbulent leakage flow. Stability characteristics are analyzed numerically for a variety of configurations. It is found that simply supported rods may become unstable at a certain critical flow speed by either divergence or flutter, depending on dimensions and fluid/solid properties. It is furthermore found that the critical flow speed is quite insensitive to use of a laminar friction model at high Reynolds numbers in cases of divergence, but sensitive to it in cases of flutter. These findings are verified analytically though analysis of an energy equation. This equation shows that (i) divergence instability is independent of fluid friction; (ii) flutter instability is caused solely by fluid friction. It also suggests a possible explanation to the question of why a 'wrong' fluid friction assumption gives a too large critical flow speed in cases of flutter instability at a high Reynolds number.

Keywords: Stability; Leakage-flow; Divergence; Flutter; Energy balance; Travelling wave

1. Introduction

A cylindrical rod in a narrow annulus is a common component in power-generation engineering. It may also serve as a model of a high-speed train in a tunnel (Sugimoto, 1996; Tanaka et al., 2001). The fluid flow within the narrow gap may initiate flutter (unstable oscillations) or divergence (buckling). It is characteristic for this and related leakage-flow problems that the rod-annulus geometry facilitates significant simplifications of the Navier–Stokes equations, but the (unsteady) inertia forces and the viscous forces have both a major influence on the dynamics and the stability properties of the structure, so neither potential theory nor lubrication theory is sufficient in itself.

The model problems which have been studied so far may roughly be separated into two classes: (i) a flexibly mounted *rigid* cylinder (or plate) in a fixed, rigid outer cylinder (or duct); (ii) a *flexible* cylinder (or plate) in a fixed, rigid outer

*Corresponding author. Tel.: +81 238 26 3326; fax: +81 238 26 3205.
E-mail address: mikael@yz.yamagata-u.ac.jp (M.A. Langthjem).

0889-9746/$ - see front matter © 2006 Elsevier Ltd. All rights reserved.
doi:10.1016/j.jfluidstructs.2006.03.002

Nomenclature

A	vibration amplitude
c	nondimensional structural damping coefficient
$\mathbf{C}$	damping matrix
D	structural displacement
$\mathscr{D}$	rate of work (power) by damping forces
e	nondimensional offset
E	modulus of elasticity
E^*	coefficient of viscoelastic material damping
$\mathscr{E}$	equilibrium offset
f	nondimensional, unsteady fluid force per unit rod length
ΔF	unsteady fluid force per unit rod length
$\mathbf{F}$	fluid-structure coupling matrix
h	nondimensional, unsteady fluid gap
h_0	nondimensional structural displacement
H	fluid gap
I	area moment of inertia
k	nondimensional structural stiffness parameter
$\mathbf{K}$	stiffness matrix
L	length of the rod
m	nondimensional structural mass parameter
M	structural mass per unit length
$\mathbf{M}$	mass matrix
$\mathbf{N}$	finite element shape function vector
p	nondimensional pressure
P	pressure
$\mathscr{P}$	rate of work (power) by fluid friction forces
q_x, q_y	nondimensional flow rate in circumferential (x) and axial (y) direction
Q_X, Q_Y	flow rate in circumferential (x) and axial (y) direction, respectively
R_0	external radius of rod
Re	Reynolds number
R_i	internal radius of hollow rod
s_t, s_r	nondimensional translational and rotational stiffness coefficient, respectively
S_T, S_R	translational and rotational stiffness coefficient, respectively
$\mathbf{S}$	fluid loading matrix
t	time
T	period of oscillation
$\mathscr{T}$	kinetic energy
U, V	flow velocity in circumferential and axial direction, respectively
$\bar{V}$	mean flow speed in axial direction
$\mathscr{V}$	potential energy
$\mathscr{W}$	work
x, y	nondimensional circumferential and axial coordinate, respectively
X, Y, Z	circumferential, axial, and radial coordinate, respectively
α	nondimensional friction parameter
β	nondimensional friction parameter related to the case of laminar flow only
δ_{ij}	Kronecker delta, $\delta_{ij} = 1$ for $i = j$; 0 for $i \neq j$
ε	nondimensional radius-to-length ratio
$\varepsilon_1, \ldots, \varepsilon_9$	nondimensional offset parameters
ζ	nondimensional local element variable
θ	nondimensional circumferential coordinate (same meaning as x)
κ	wave number
λ	friction factor defined by (6)
Λ	complex eigenvalue

ν	kinematic viscosity
ξ_{in}, ξ_{ex}	inlet and exit pressure loss coefficient, respectively
Ξ	a nondimensional parameter defined by (18)
ρ	fluid density
τ	nondimensional time
ϕ	phase angle
ω	nondimensional cyclic frequency
Ω	dimensional cyclic frequency

cylinder (or duct). Early studies of class (i) problems were reviewed by Mulcahy (1980). More recent, general reviews are Païdoussis (1996) and Weaver et al. (2000). Païdoussis's (2004) monograph contains a comprehensive (200 pages) and wide-ranging review of the entire subject. An example of a recent class (i) study is Li et al. (2002) who investigated the stability of a flexibly mounted rigid cylinder in a rigid outer cylinder, allowing for offset (from the axis of the outer cylinder) of the inner cylinders equilibrium.

The problem studied in the present work belongs to class (ii). Papers in this class are relatively few. The stability of a flexible cylinder in a narrow coaxial duct with flow was studied by Païdoussis and Pettigrew (1979), Païdoussis et al. (1990), Fujita and Shintani (2001), and Fujita et al. (2004). The stability of a flexible plate in a narrow rigid duct with flow was studied by Inada (1999), Inada and Hayama (2000), and Inada (2004). Kaneko et al. (2000) and Wu and Kaneko (2005) applied a similar model to explain sheet flutter observed in paper manufacturing machines and in the production of steel plates.

The mentioned studies of Inada (1999), Inada and Hayama (2000), Inada (2004), Li et al. (2002), Fujita and Shintani (2001), Fujita et al. (2004), Kaneko et al. (2000), and Wu and Kaneko (2005) are all based on the (plane, 2-D) leakage-flow model of Inada and Hayama (1990). This model uses flow rates rather than flow velocities, an approach that simplifies the underlying Navier–Stokes equations in a very efficient way. It accounts for both laminar and turbulent flows via employment of a friction coefficient, as known from engineering analysis of pipe and duct flows [e.g., Fox and McDonald (1985)].

The 2-D analyses of Kaneko et al. (2000) and Wu and Kaneko (2005) thus also account for both laminar and turbulent flows. But in the axisymmetric problems studied by Li et al. (2002), Fujita and Shintani (2001), and Fujita et al. (2004) the models are restricted to laminar flow only. Most industrial flows of Newtonian fluids (like air and water) are however turbulent, and it is obviously not too reassuring to apply a laminar flow model to highly turbulent flows. In the present paper the mentioned earlier studies are developed to account for turbulent flow, and results obtained with laminar and turbulent models are compared. It is noted that a 'bulk-flow theory for turbulence in lubricant films' has been developed by Hirs (1973). This is a lubrication theory (where the fluid inertia is neglected) given in terms of average flow velocities. The friction terms in the equations derived in the present paper agree with those of Hirs.

Another extension is the inclusion of offset of the equilibrium position from the annulus symmetry axis (eccentricity). This is also of practical interest, because perfect alignment of the inner cylinder is difficult, and nonconservative (circulatory) systems, like the present, are often sensitive to imperfections (Herrmann, 1971; Langthjem and Sugiyama, 2000).

The 'idealized' case with assumptions of laminar flow and perfect alignment (no eccentricity) makes elimination of the flow rate perturbations possible, leaving the structural deflection as the only unknown (Fujita and Shintani, 2001). Such a simplification is not possible in the more general setting considered here. The axial flow rate perturbation must also be explicitly determined, in addition to the structural deflection. [The circumferential flow rate perturbation is then obtained from the continuity equation.]

It must be emphasized that determination of the axial flow rate perturbation also is necessary for a correct analysis of cases with moving rod ends, even if laminar flow and perfect alignment is assumed, at least if Inada and Hayama's (1990) fluid boundary conditions are adopted. This is because these boundary conditions express, in fact, a turbulent pressure loss. They have a form analogous to 'minor head loss' expressions for turbulent flow in pipes, as described in books on engineering fluid dynamics.

The analysis of this paper gives a system of coupled fluid-structure differential equations with, as mentioned, the structural deflection and the axial flow rate perturbation as unknowns. These equations are discretized using the Galerkin finite element method (in the form sometimes called the Bubnov–Galerkin method (Cook et al., 1989)). It is worthwhile noting that the Galerkin finite element method is completely equivalent to the 'classical' Galerkin weighted residual method (based on global expansion functions), and the latter method could just as well have been used in the

present context. The advantage of the finite element form of Galerkin's method is that various boundary (rod support) conditions and 'asymmetries' (such as, for example, partial immersion) can be taken into consideration in a very simple way, since the (local, element) expansion functions are chosen 'once and for all'.

Li et al. (2002) use a collocation method to determine both the axial and the circumferential flow rate perturbation. Their approach could also have been applied to the present problem including a flexible rod; we think, however, that the Galerkin finite element-based approach of this paper is simpler.

It is remarked that a formulation of fluid boundary conditions for movable rod ends that does not require explicit evaluation of the axial flow rate perturbation can be achieved through consideration of a shear force balance in the way of Hawthorne (1961) and Païdoussis (1966). But still, with the structural deflection as the only unknown, only laminar flow can be considered.

The paper is divided into 10 sections. In Section 2 equations of motion are given for a laminar and, in particular, a turbulent leakage flow, and for a Bernoulli–Euler rod. In Section 3 these equations are made nondimensional. In Section 4 it is discussed how the fluid equations can be simplified. In Section 5 the fluid force acting on the rod is evaluated. In Section 6 the discretization of the fluid and solid equations of motion is discussed. In Section 7 an eigenvalue problem for dynamic stability analysis is formulated. In Section 8 some numerical results are presented and discussed. The main findings are that (i) a simply supported rod may become unstable by either divergence or flutter, depending on dimensions and fluid/solid properties; (ii) the critical flow speed where a *divergence* instability is initiated is quite insensitive to use of a laminar friction model at high Reynolds numbers; (iii) the critical flow speed where a *flutter* instability is initiated is, on the contrary, sensitive to a 'wrong' flow model assumption. In Section 9 a detailed analysis of these findings is carried out through an energy balance study. This study is able to explain points (i)–(iii) outlined above. Section 10 sums up the main conclusions. The final part of the paper includes five appendices with mathematical details.

2. Equations of motion and boundary conditions

2.1. Fluid equations of motion

Consider an incompressible flow through a narrow gap of clearance H between coaxial cylinders of length L, of which the inner cylinder has radius R_0 (Fig. 1(a)). Assuming that $H \ll R_0$, $H \ll L$, Li et al. (2002) argue that the relations between pressure P, flow rate in circumferential (X) direction Q_X, and flow rate in axial (Y) direction Q_Y, can be expressed as

$$\frac{1}{\rho}\frac{\partial P}{\partial X} = -\frac{1}{H}\left\{\frac{\partial Q_X}{\partial t} + \frac{\partial}{\partial X}\left(\frac{Q_X^2}{H}\right) + \frac{\partial}{\partial Y}\left(\frac{Q_X Q_Y}{H}\right) + \frac{\lambda}{4}\frac{(Q^2)_X}{H^2}\right\}, \tag{1}$$

$$\frac{1}{\rho}\frac{\partial P}{\partial Y} = -\frac{1}{H}\left\{\frac{\partial Q_Y}{\partial t} + \frac{\partial}{\partial X}\left(\frac{Q_X Q_Y}{H}\right) + \frac{\partial}{\partial Y}\left(\frac{Q_Y^2}{H}\right) + \frac{\lambda}{4}\frac{(Q^2)_Y}{H^2}\right\}, \tag{2}$$

$$\frac{\partial Q_X}{\partial X} + \frac{\partial Q_Y}{\partial Y} + \frac{\partial H}{\partial t} = 0, \tag{3}$$

where t is the time and $X = \theta R_0$, $0 \leqslant \theta \leqslant 2\pi$, see Fig. 1. The flow rates Q_X and Q_Y are defined as (Inada and Hayama, 1990)

$$Q_X(X, Y, t) = \int_0^H U(X, Y, Z, t)\,\mathrm{d}Z,$$

$$Q_Y(X, Y, t) = \int_0^H V(X, Y, Z, t)\,\mathrm{d}Z, \tag{4}$$

where U and V are the flow velocities in the X and Y direction, respectively. Q^2 is the total flow rate squared, given by $Q^2 = Q_X^2 + Q_Y^2$; $(Q^2)_X$ and $(Q^2)_Y$ are the projections of Q^2 onto the X and Y direction, respectively. Let ψ be the angle between the flow direction and the Y-axis. Then $(Q^2)_X = Q^2 \sin\psi$ and $(Q^2)_Y = Q^2 \cos\psi$. Since $\sin\psi = Q_X/Q$ and $\cos\psi = Q_Y/Q$,

$$(Q^2)_X = QQ_X, \quad (Q^2)_Y = QQ_Y. \tag{5}$$

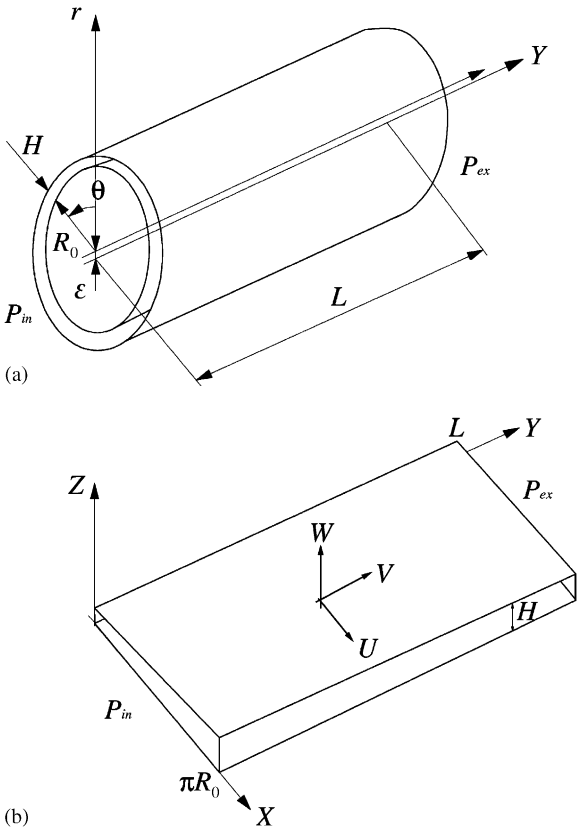

Fig. 1. (a) Definition sketch of coordinates and symbols of the physical system. An elastic rod of length L and external radius R_0 is immersed in an annulus with fluid gap H. The fluid flow is thought to be initially described in cylindrical polar coordinates (Y, θ, r). The stable equilibrium of the rod is offset from the centre axis by the distance $\mathscr{E}$. Fluid pressures a little before the annulus entrance and a little after the annulus exit are denoted by P_{in} and P_{ex}, respectively. (b) Definition sketch of coordinates and symbols used in the small-gap approximation. When the fluid gap is small, the curvature of the fluid channel is insignificant, and the fluid flow within the gap is effectively equivalent to the flow within two plates of dimension $2\pi R_0 \times L$ (of which half is shown), described in terms of rectangular coordinates (X, Y, Z). The flow velocities in these directions are U, V, and W, respectively. They are, by integration over the gap, replaced by the flow rates Q_X and Q_Y, and the gap rate-of-change $\partial H/\partial t$.

Inserting (5) into (1) and (2), it may be confirmed that the fluid friction parts (the last terms) are in agreement with Eqs. (7a)–(7b) of Hirs (1973).

The main assumption of Li et al. for the development of (1)–(3) is, as indicated above, that the fluid gap is so narrow, relative to the radius and the length of the inner cylinder, that the flow there resembles a boundary layer. This implies that (i) the pressure difference across the gap (in the radial (Z) direction) is negligibly small, (ii) the effect of curvature can be ignored [see, e.g., Schlichting (1968), pp. 223–224]. The fluid flow within the gap is thus, effectively, equivalent to the flow within two plates (Fig. 1(b)).

As discussed in the Introduction, a difference between (1) and (2) and the corresponding equations in Li et al. (2002), and in Fujita and Shintani (2001), is that (1) and (2) include both laminar and turbulent flow (included in the friction factor λ), while Li et al. and Fujita and Shintani assume laminar flow only. The derivation of both laminar and turbulent friction terms is given in Appendix A.

The value of the friction factor λ follows the experimental results of Shimoyama and Yamada (1957) for coaxial, smooth cylinders with very small clearance:

$$\lambda = \begin{cases} 48\text{Re}^{-1} & \text{for Re} < 1300 \text{ (laminar flow)}, \\ 0.26\text{Re}^{-0.24} & \text{for Re} > 2000 \text{ (turbulent flow)}, \end{cases} \tag{6}$$

where the Reynolds number Re is defined as

$$\mathrm{Re} = Q/v. \tag{7}$$

Shimoyama and Yamada (1957) write that *fully developed* turbulence ensues for $\mathrm{Re} > 2500$. In the domain $1300 < \mathrm{Re} < 2000$ the value of λ is characterized by strong scatter (see Fig. 3 in their paper). [Shimoyama and Yamada (1957) mention just that $\lambda \approx 0.035 \sim 0.041$ in this domain; it cannot be defined more precisely.] The scatter in the domain $2000 < \mathrm{Re} < 2500$ is much more limited. Based on this it is thought reasonable to assume that the flow is turbulent from $\mathrm{Re} = 2000$. In the transition domain $1300 < \mathrm{Re} < 2000$, the friction factor (not Eq. (6) directly, but its steady part, to be defined by Eq. (11)) is simply interpolated linearly between the laminar and turbulent values. [This has no physical meaning, but is done solely to avoid discontinuities in the eigenvalue plots (Section 8), such that the evolution of the individual eigenvalues can be followed.]

2.2. Fluid boundary conditions

By making use of the Bernoulli and momentum equations, the fluid boundary conditions, applying at $Y = 0$ and $Y = L$, are obtained as (Inada and Hayama, 1990)

$$P(X,0,t) = P_{\mathrm{in}} - (1+\xi_{\mathrm{in}})\frac{\rho}{2}\frac{(Q^2(X,0,t))_Y}{H^2(X,0,t)}, \tag{8}$$

$$P(X,L,t) = P_{\mathrm{ex}} + \xi_{\mathrm{ex}}\frac{\rho}{2}\frac{(Q^2(X,L,t))_Y}{H^2(X,L,t)}.$$

Here P_{in} is the mean pressure a little before the annulus entrance, and P_{ex} is the mean pressure a little behind the annulus exit; ρ is the fluid density. The inlet loss coefficient ξ_{in} accounts for the formation of a 'vena contracta' just after the inlet. Books on engineering fluid dynamics give, for pipe flow with a contraction, that ξ_{in} typically is in the range between 0 and 0.5. As to the exit flow, $\xi_{\mathrm{ex}} = 0$ corresponds to an abrupt channel enlargement where all kinetic energy is lost. Values $\xi_{\mathrm{ex}} > 0$ correspond to additional pressure losses, for example due to a small contraction before the exit.

2.3. Linearization of the fluid equations

The fluid gap H, the pressure P, and the flow rates Q_X and Q_Y are separated into steady (constant) parts (with a bar) and unsteady (disturbance) parts (with a Δ) (Inada and Hayama, 1990)

$$H(X,Y,t) = \bar{H} + \Delta H(X,Y,t), \quad P(X,Y,t) = \bar{P} + \Delta P(X,Y,t), \tag{9}$$

$$Q_X(X,Y,t) = \Delta Q_X(X,Y,t), \quad Q_Y(X,Y,t) = \bar{Q}_Y + \Delta Q_Y(X,Y,t).$$

It should be noticed that the steady part of the circumferential flow rate, $\bar{Q}_X$, is assumed to be zero. This is considered reasonable for small-amplitude vibrations, as assumed here; Q_X is then much smaller than the axial flow rate Q_Y. As linear stability is to be investigated, only terms of first order in the small disturbances $\Delta P, \Delta Q_X, \Delta Q_Y, \Delta H$ are kept. The influence of the (first order) fluctuations in Q_Y on the friction coefficient λ is included as (Inada and Hayama, 1990)

$$\lambda = \bar{\lambda} + \Delta\lambda = \bar{\lambda} + \left[\frac{\partial\lambda}{\partial Q_Y}\right]_{(Q_X,Q_Y)=(0,\bar{Q}_Y)} \Delta Q_Y, \tag{10}$$

where

$$\bar{\lambda} = \begin{cases} 48\overline{\mathrm{Re}}^{-1}, & \overline{\mathrm{Re}} < 1300, \\ 0.26\overline{\mathrm{Re}}^{-0.24}, & \overline{\mathrm{Re}} > 2000, \end{cases} \quad \overline{\mathrm{Re}} = \bar{Q}_Y/v. \tag{11}$$

[A term $[\partial\lambda/\partial Q_X]_{(Q_X,Q_Y)=(0,\bar{Q}_Y)}\Delta Q_X$ is basically also to be included on the right-hand side of (10), but it is zero since the steady part of Q_X is assumed to be zero.] Evaluation of (10) gives

$$\lambda = \begin{cases} 48\overline{\mathrm{Re}}^{-1}\left(1 - \dfrac{\Delta Q_Y}{\bar{Q}_Y}\right), & \overline{\mathrm{Re}} < 1300, \\ 0.26\overline{\mathrm{Re}}^{-0.24}\left(1 - 0.24\dfrac{\Delta Q_Y}{\bar{Q}_Y}\right), & \overline{\mathrm{Re}} > 2000. \end{cases} \tag{12}$$

Negative powers of the gap H are expanded as

$$H^{-1} = (\bar{H} + \Delta H)^{-1} = \bar{H}^{-1} - \bar{H}^{-2}\Delta H + \mathcal{O}(\Delta H^2),$$

$$H^{-2} = \bar{H}^{-2} - 2\bar{H}^{-3}\Delta H + \mathcal{O}(\Delta H^2), \quad H^{-3} = \bar{H}^{-3} - 3\bar{H}^{-4}\Delta H + \mathcal{O}(\Delta H^2). \tag{13}$$

Expanding (5) and keeping only the steady part and first-order disturbance-parts, we obtain (see Appendix B)

$$(Q^2)_X \approx \bar{Q}_Y \Delta Q_X, \quad (Q^2)_Y \approx \bar{Q}_Y^2 + 2\bar{Q}_Y \Delta Q_Y. \tag{14}$$

Using (9) and (11)–(14), the unsteady parts of (1), (2) and (3) can, to first order in the disturbances, be written as

$$\frac{1}{\rho}\frac{\partial \Delta P}{\partial X} = -\frac{1}{\bar{H}}\left\{\frac{\partial \Delta Q_X}{\partial t} + \frac{\bar{Q}_Y}{\bar{H}}\frac{\partial \Delta Q_X}{\partial Y}\right\} - \frac{\bar{\lambda}}{4}\frac{\bar{Q}_Y}{\bar{H}^3}\Delta Q_X, \tag{15}$$

$$\frac{1}{\rho}\frac{\partial \Delta P}{\partial Y} = -\frac{1}{\bar{H}}\left\{\frac{\partial \Delta Q_Y}{\partial t} + \frac{\bar{Q}_Y}{\bar{H}}\left(\frac{\partial \Delta Q_Y}{\partial Y} - \frac{\partial \Delta H}{\partial t}\right) - \frac{\bar{Q}_Y^2}{\bar{H}^2}\frac{\partial \Delta H}{\partial Y}\right\} - \frac{\bar{\lambda}}{4}\frac{\bar{Q}_Y}{\bar{H}^3}\left\{(1+\Xi)\Delta Q_Y - 3\frac{\bar{Q}_Y}{\bar{H}}\Delta H\right\}, \tag{16}$$

$$\frac{\partial \Delta Q_X}{\partial X} + \frac{\partial \Delta Q_Y}{\partial Y} + \frac{\partial \Delta H}{\partial t} = 0. \tag{17}$$

The coefficient Ξ appearing in the friction term in (16) is given by

$$\Xi = \begin{cases} 0 & \text{for } \overline{\mathrm{Re}} < 1400, \\ 0.76 & \text{for } \overline{\mathrm{Re}} > 2000. \end{cases} \tag{18}$$

The resulting factor 1.76 ($= 1 + \Xi$) in (16), in the turbulent case, comes from linearization of the term $\frac{1}{4}\lambda Q Q_y / H^3$; (details are given in Appendix B). Similar to the steady friction factor $\bar{\lambda}$, Ξ is taken to vary linearly between 0 and 0.76 in the transition domain $1300 < \overline{\mathrm{Re}} < 2000$ (and the same comments apply to the reasons for doing this).

The corresponding steady parts to (15)–(17) can, together with the structural force balance Eq. (23) (see Section 2.5), be used to determine the position of stable equilibrium. Here we assume that this is $Y \equiv \mathscr{E}$, where $\mathscr{E}$ is a possible offset (see Section 2.4). Accordingly, the steady equivalents of (15)–(17) are not used.

By linearization, the unsteady boundary conditions (8) become

$$\Delta P = -(1 + \xi_{\mathrm{in}})\rho \frac{\bar{Q}_Y^2}{\bar{H}^2}\left(\frac{\Delta Q_Y}{\bar{Q}_Y} - \frac{\Delta H}{\bar{H}}\right) \quad \text{at } Y = 0, \tag{19}$$

$$\Delta P = \xi_{\mathrm{ex}}\rho \frac{\bar{Q}_Y^2}{\bar{H}^2}\left(\frac{\Delta Q_Y}{\bar{Q}_Y} - \frac{\Delta H}{\bar{H}}\right) \quad \text{at } Y = L.$$

Finally, for later use, we will at this place also define the mean flow speed in the Y direction, $\bar{V}$, as

$$\bar{V} = \bar{Q}_Y / \bar{H}. \tag{20}$$

2.4. Modifications due to equilibrium offset

When the equilibrium of the rod is offset a distance $\mathscr{E}$ from the centre axis, the steady gap $\bar{H}$ is not a constant but a function of X (Li et al. (2002), Eq. (17)):

$$\bar{H} = \bar{H}(X) = \bar{H}_0 - \mathscr{E}\cos(X/R_0), \tag{21}$$

where $\bar{H}_0$ is a constant. Going back to (1) and (2) it will be seen that no modifications are introduced in (15). But in (16) the additional term

$$\frac{\bar{Q}_Y}{\bar{H}^3}\frac{\mathscr{E}}{R}\sin(X/R_0)\Delta Q_X \tag{22}$$

must be added to the right-hand side. This is in agreement with Li et al. (2002), Eqs. (20)–(22).

2.5. Equation of motion and boundary conditions for the rod

It is assumed that the rod vibrates only in the plane $X = 0$ ($\theta = 0$; see Fig. 1). It is furthermore assumed that the rod is sufficiently slender, and the vibrations of sufficiently low frequency, that shear deformation and rotatory inertia can be neglected. Kelvin–Voigt type structural damping is taken into consideration. The equation of motion is then given by (Païdoussis, 1998)

$$M\frac{\partial^2 D}{\partial t^2} + E^* I\frac{\partial^5 D}{\partial Y^4 \partial t} + EI\frac{\partial^4 D}{\partial Y^4} = \Delta F, \tag{23}$$

where $D(Y,t)$ is the displacement in the plane $X = 0$, M is the structural mass per unit length, E is the modulus of elasticity, E^* is the coefficient of material damping (viscoelastic resistance), I is the area moment of inertia, and $\Delta F(Y,t)$ is the unsteady fluid force per unit length.

General boundary conditions, covering any set of standard boundary conditions, can be specified as (Païdoussis, 1973)

$$EI\frac{\partial^2 D}{\partial Y^2} + E^* I\frac{\partial^3 D}{\partial Y^2 \partial t} - S_{R0}\frac{\partial D}{\partial Y} = 0, \quad EI\frac{\partial^3 D}{\partial Y^3} + E^* I\frac{\partial^4 D}{\partial Y^3 \partial t} + S_{T0} D = 0, \quad \text{at } Y = 0,$$

$$EI\frac{\partial^2 D}{\partial Y^2} + E^* I\frac{\partial^3 D}{\partial Y^2 \partial t} + S_{RL}\frac{\partial D}{\partial Y} = 0, \quad EI\frac{\partial^3 D}{\partial Y^3} + E^* I\frac{\partial^4 D}{\partial Y^3 \partial t} - S_{TL} D = 0, \quad \text{at } Y = L, \tag{24}$$

where S_{T0}, S_{TL} are translational, and S_{R0}, S_{RL} rotational, springs constants at $Y = 0$ and L, respectively. A rod clamped at $Y = 0$ and free at $Y = L$, for example, is obtained by letting $S_{R0} = S_{T0} = \infty$ and $S_{RL} = S_{TL} = 0$. [This, however, is not used directly in the finite element analysis in Section 6. Zero displacement/rotation boundary conditions are implemented in exact form, in order to avoid an ill-conditioned matrix system.]

3. Nondimensionalization

To recast the governing equations into nondimensional form, the following nondimensional parameters are introduced.

Fluid parameters:

$$x = \frac{X}{R_0}, \quad h = \frac{\Delta H}{\widetilde{H}}, \quad \bar{h} = \frac{\bar{H}}{\widetilde{H}}, \quad \bar{h}_0 = \frac{\bar{H}_0}{\widetilde{H}}, \quad e = \frac{\mathscr{E}}{\widetilde{H}}, \quad \varepsilon = \frac{R_0}{L},$$

$$p = \frac{\Delta P}{\rho\widetilde{Q}^2/\widetilde{H}^2}, \quad q_x = \frac{\Delta Q_X}{\widetilde{Q}}, \quad q_y = \frac{\Delta Q_Y}{\widetilde{Q}}, \quad \bar{q}_y = \frac{\bar{Q}_Y}{\widetilde{Q}}, \quad \alpha = \frac{\lambda L}{4\widetilde{H}}, \quad \beta = \frac{12\nu L}{\widetilde{Q}\widetilde{H}}. \tag{25}$$

Structural parameters:

$$m = \frac{M}{M_0}, \quad c = \frac{E^* I\widetilde{H}}{M_0 L^3\widetilde{Q}}, \quad k = \frac{EI\widetilde{H}^2}{M_0 L^2\widetilde{Q}^2}, \quad f = \Delta F\frac{\widetilde{H}L^2}{M_0\widetilde{Q}^2},$$
$$h_0 = \frac{D}{\widetilde{H}}, \quad s_t = S_T\frac{\widetilde{H}^2 L}{M_0\widetilde{Q}^2}, \quad s_r = S_R\frac{\widetilde{H}^2}{M_0 L\widetilde{Q}^2}. \tag{26}$$

Common parameters:

$$y = \frac{Y}{L}, \quad \tau_* = \frac{\widetilde{H}L}{\widetilde{Q}}, \quad \tau = \frac{t}{\tau_*}. \tag{27}$$

Here $M_0 = \rho\pi R_0^2$. $\widetilde{H}$ is a reference gap and $\widetilde{Q}$ a reference flow rate, both of which can be chosen freely ($\neq 0$). The final equations are simplified by choosing $\widetilde{H} = \bar{H}_0$, such that $\bar{h}_0 = 1$, see (45)–(47), but it is thought useful to keep $\bar{h}_0$ in these equations for future developments involving, e.g., nonconstant mean fluid gap [such as considered by Li et al. (2002)].

Li et al. (2002) take $\widetilde{Q}$ to be the variable $\bar{Q}_Y$ (the axial mean flow rate), such that $\bar{q}_y = 1$. But then the parameters with $\widetilde{Q}$ in the denominator will be undefined for $\bar{Q}_Y = 0$. It is numerically more convenient to keep $\bar{q}_y$ as an independent

flow-rate parameter, by defining $\widetilde{Q}$ as a constant, e.g.

$$\widetilde{Q} = \frac{\bar{H}_0}{L}\left(\frac{EI}{M_0}\right)^{1/2}. \tag{28}$$

Reduction of the parameters in (25)–(26) by use of (28) is straightforward and will not be shown here.

The nondimensional governing fluid equations, with modification for equilibrium offset (22) included, are

$$\frac{\partial p}{\partial x} = -\varepsilon\left\{\frac{1}{\bar{h}}\frac{\partial q_x}{\partial \tau} + \frac{\bar{q}_y}{\bar{h}^2}\frac{\partial q_x}{\partial y} + \frac{\alpha}{\bar{h}^3}\bar{q}_y q_x\right\}, \tag{29}$$

$$\frac{\partial p}{\partial y} = -\frac{1}{\bar{h}}\frac{\partial q_y}{\partial \tau} - \frac{\bar{q}_y}{\bar{h}^2}\frac{\partial q_y}{\partial y} + \frac{\bar{q}_y}{\bar{h}^2}\frac{\partial h}{\partial \tau} + \frac{\bar{q}_y^2}{\bar{h}^3}\frac{\partial h}{\partial y} - \frac{\alpha}{\bar{h}^3}\left\{(1+\Xi)\bar{q}_y q_y - \frac{3\bar{q}_y^2}{\bar{h}}h\right\} + \frac{1}{\varepsilon}\frac{e}{\bar{h}^3}\bar{q}_y q_x \sin x, \tag{30}$$

$$\frac{\partial q_x}{\partial x} + \varepsilon\left\{\frac{\partial q_y}{\partial y} + \frac{\partial h}{\partial \tau}\right\} = 0. \tag{31}$$

The corresponding boundary conditions are

$$p = -(1+\xi_{\text{in}})\frac{\bar{q}_y}{\bar{h}^2}\left(q_y - \frac{\bar{q}_y}{\bar{h}}h\right) \quad \text{at } y = 0,$$

$$p = \xi_{\text{ex}}\frac{\bar{q}_y}{\bar{h}^2}\left(q_y - \frac{\bar{q}_y}{\bar{h}}h\right) \quad \text{at } y = 1. \tag{32}$$

The nondimensional equation of motion for the rod is

$$m\frac{\partial^2 h_0}{\partial \tau^2} + c\frac{\partial^5 h_0}{\partial y^4 \partial \tau} + k\frac{\partial^4 h_0}{\partial y^4} = f. \tag{33}$$

The corresponding boundary conditions are

$$k\frac{\partial^2 h_0}{\partial y^2} - s_{r0}\frac{\partial h_0}{\partial y} = 0, \quad k\frac{\partial^3 h_0}{\partial y^3} + s_{t0}h_0 = 0 \quad \text{at } y = 0,$$

$$k\frac{\partial^2 h_0}{\partial y^2} + s_{r1}\frac{\partial h_0}{\partial y} = 0, \quad k\frac{\partial^3 h_0}{\partial y^3} - s_{t1}h_0 = 0 \quad \text{at } y = 1. \tag{34}$$

Finally, it is noted that for the gap with offset, the steady part (21) can be written in nondimensional form as

$$\bar{h} = \bar{h}(x) = \bar{h}_0 - e\cos x. \tag{35}$$

4. Simplification of the fluid equations

4.1. Dependence on the circumferential coordinate x

The rod deflection in circumferential direction x is given $h_0 \cos x$, $0 \leqslant x \leqslant 2\pi$, see Fig. 1. Due to the narrow gap geometry, the unsteady gap varies in the same way (Li et al., 2002, Eq. (18)), i.e.,

$$h(x, y, \tau) = h_0(y, \tau)\cos x. \tag{36}$$

From (31) it is seen that this also applies to the axial flow rate q_y perturbation,

$$q_y(x, y, \tau) = q_{y0}(y, \tau)\cos x, \tag{37}$$

and that the circumferential flow rate perturbation q_x varies with x as

$$q_x = -\varepsilon\left(\frac{\partial q_{y0}}{\partial y} + \frac{\partial h_0}{\partial \tau}\right)\sin x. \tag{38}$$

The x-momentum equation (29) shows that the perturbation pressure p then also varies harmonically with x, i.e., we have (Fujita and Shintani, 2001)

$$p = -\frac{\partial^2 p}{\partial x^2}. \tag{39}$$

4.2. Elimination of q_x

It is necessary to solve the coupled system (29)–(31) and (33)–(34) for the unsteady fluid gap h, and the axial flow rate perturbation q_y, in order to take the boundary conditions (32) into consideration. But information concerning the circumferential flow rate perturbation q_x are not needed. This function may thus be eliminated. Using (36)–(39) in (29) and (30) gives, after differentiation of (29) with respect to x,

$$-p = \varepsilon^2 \left\{ \left(\frac{1}{\bar{h}} \cos x - \frac{1}{\bar{h}^2} e \sin^2 x \right) \left(\frac{\partial^2 h_0}{\partial \tau^2} + \frac{\partial^2 q_{y0}}{\partial y \partial \tau} \right) + \left(\frac{1}{\bar{h}^2} \cos x - \frac{2}{\bar{h}^3} e \sin^2 x \right) \bar{q}_y \left(\frac{\partial^2 h_0}{\partial y \partial \tau} + \frac{\partial^2 q_{y0}}{\partial y^2} \right) + \alpha \bar{q}_y \left(\frac{1}{\bar{h}^3} \cos x - \frac{3}{\bar{h}^4} e \sin^2 x \right) \left(\frac{\partial h_0}{\partial \tau} + \frac{\partial q_{y0}}{\partial y} \right) \right\}, \tag{40}$$

$$\frac{\partial p}{\partial y} = \left(\frac{1}{\bar{h}^2} \cos x - \frac{1}{\bar{h}^3} e \sin^2 x \right) \bar{q}_y \frac{\partial h_0}{\partial \tau} - \frac{1}{\bar{h}} \cos x \frac{\partial q_{y0}}{\partial \tau} - \left(\frac{1}{\bar{h}^2} \cos x + \frac{1}{\bar{h}^3} e \sin^2 x \right) \bar{q}_y \frac{\partial q_{y0}}{\partial y} + \frac{\bar{q}_y^2}{\bar{h}^3} \cos x \frac{\partial h_0}{\partial y} + \alpha \cos x \left(\frac{3}{\bar{h}^4} \bar{q}_y^2 h_0 - \frac{1 + \Xi}{\bar{h}^3} \bar{q}_y q_{y0} \right). \tag{41}$$

4.3. Elimination of q_y as well for a special case

Further simplification of (40) and (41) is possible if (i) the rod is at least simply supported at both ends; (ii) the flow is laminar; (iii) there is no offset of the equilibrium. Condition (i) implies that the fluid boundary conditions reduce to $p = 0$ at $y = 0, 1$. Accordingly, information concerning the axial flow q_y rate is not necessary either, and may be eliminated. Condition (ii) implies that $\alpha = \beta$ and $\Xi = 0$. Condition (iii) implies that $e = 0$. Inserting these values in (40) and (41), followed by differentiation of (41) with respect to y, and addition of the two equations, a single equation in p and h_0 is obtained as

$$\varepsilon^2 \frac{\partial^2 p}{\partial y^2} - p = \varepsilon^2 \left[\frac{1}{\bar{h}} \frac{\partial^2 h_0}{\partial \tau^2} + \frac{2 \bar{q}_y}{\bar{h}^2} \frac{\partial^2 h_0}{\partial y \partial \tau} + \frac{\beta}{\bar{h}^3} \frac{\partial h_0}{\partial \tau} + \beta \frac{3 \bar{q}_y}{\bar{h}^4} \frac{\partial h_0}{\partial y} + \frac{1}{\bar{h}^3} \frac{\partial^2 h_0}{\partial y^2} \right] \cos x, \tag{42}$$

where (39) has been used to obtain the second term on the left-hand side. Relating (42) to the rod equation (33), the left-hand side acts as the forcing term f (see Section 5). The terms on the right-hand side have the following physical meanings. The first term is an inertia force due to added fluid mass. The second term is a Coriolis force due to the movement of fluid mass in the deformed (curved) gap. The third term is a viscous damping force. The fourth term is a nonconservative (tangential, or 'follower'-type) viscous force. The fifth term is compressive 'moving load-type' force (or 'centrifugal force'), conservative or nonconservative depending on the structural boundary conditions.

It is noted that Fujita and Shintani (2001) give an equation similar to (42), but in symbolic (non-explicit) form, and without the first term on the left-hand side (Eq. (10) in their paper). Although ε is a small parameter (see (25)) it is not clear at this point whether this term can be neglected, as the right-hand side also is multiplied by ε^2. But by evaluating the resultant fluid force acting on the rod, by integrating the fluid pressure over the rod surface (see the following section) it will become clear that the first term (left-hand side) in fact is small in comparison with the second (see (58) in Section 9).

In the following, Eq. (42) will be used in analysis of instability mechanisms (Section 9). It will not be used in connection with numerical computations.

5. Evaluation of the fluid force acting on the rod

The resultant fluid force acting on the rod is obtain by integrating the fluid pressure over the rod surface. Let $r(x) = r_0 + e \cos x$, $r_0 = R_0/\widetilde{H}$, denote the radius of the rod, measured from the centre axis of the duct, in nondimensional form. The (nondimensional) unsteady fluid force per unit length, acting in the $x = 0$ direction, is then (Païdoussis, 1998, p. 40)

$$f(y, \tau) = \frac{\rho L^2}{M_0} \int_0^{2\pi} r(x) p(x, y, \tau) \cos x \, \mathrm{d}x. \tag{43}$$

The nondimensional factor $\rho L^2/M_0$ appears because the physical (dimensional) perturbation pressure ΔP was nondimensionalized using fluid variables, while the physical (dimensional) fluid force ΔF was nondimensionalized using structural (rod) variables; see Eqs. (25) and (26), respectively.

Eq. (43) must now be applied to the momentum equations (40)–(41) and boundary conditions (32), in order to convert the perturbation pressure $p(x, y, \tau)$ in these equations to the fluid force $f(y, \tau)$, such that they can be coupled with the structural equations (33)–(34). It is noted that, with equilibrium offset, the steady fluid gap $\bar{h}$ is not a constant but a function of x, see Eq. (35). Integration of (40), (41), and (32) over x will thus result in quite complicated expressions. To simplify the integrals, such that they can be evaluated analytically and such that the final equations are reasonably 'compact', it will be assumed that the offset e is small, $e \ll 1$. Fractions in $\bar{h}$ will then be expanded in Taylor series about $e = 0$, keeping only terms up to $\mathcal{O}(e^3)$, for example,

$$\frac{1}{\bar{h}} = \frac{1}{\bar{h}_0 - e\cos x} = \frac{1}{\bar{h}_0} + \frac{e}{\bar{h}_0^2}\cos x + \frac{e^2}{\bar{h}_0^3}\cos^2 x + \mathcal{O}(e^3). \tag{44}$$

Fig. 2 gives an indication of the range of validity of the right-hand side of (44). The upper curve depicts the function $1/(1-e)$, the lower curve its second-order Taylor expansion $1 + e + e^2$. At $e = 0.25$ the difference is 0.021∼2.1%. The error is increasing rapidly for larger values of e. In the light of Fig. 2, it is thought reasonable to consider off-sets up to $e \approx 0.25\bar{h}_0$.

Applying (43) and (44) to the momentum equations (40)–(41) and boundary conditions (32) gives

$$-f = p_0\left\{\frac{\varepsilon_1}{\bar{h}_0}\left(\frac{\partial^2 h_0}{\partial\tau^2} + \frac{\partial^2 q_{y0}}{\partial y\partial\tau}\right) + \frac{\varepsilon_2}{\bar{h}_0^2}\bar{q}_y\left(\frac{\partial^2 h_0}{\partial y\partial\tau} + \frac{\partial^2 q_{y0}}{\partial y^2}\right) + \alpha\bar{q}_y\frac{\varepsilon_3}{\bar{h}_0^3}\left(\frac{\partial h_0}{\partial\tau} + \frac{\partial q_{y0}}{\partial y}\right)\right\}, \tag{45}$$

$$\varepsilon^2\frac{\partial f}{\partial y} = p_0\left\{\frac{\varepsilon_4}{\bar{h}_0^2}\bar{q}_y\frac{\partial h_0}{\partial\tau} - \frac{\varepsilon_6}{\bar{h}_0}\frac{\partial q_{y0}}{\partial\tau} - \frac{\varepsilon_5}{\bar{h}_0^2}\bar{q}_y\frac{\partial q_{y0}}{\partial y} + \frac{\varepsilon_7}{\bar{h}_0^3}\bar{q}_y^2\frac{\partial h_0}{\partial y} + \alpha\left(3\frac{\varepsilon_8}{\bar{h}_0^4}\bar{q}_y^2 h_0 - (1+\Xi)\frac{\varepsilon_7}{\bar{h}_0^3}\bar{q}_y q_{y0}\right)\right\}, \tag{46}$$

$$\begin{aligned}
\varepsilon^2 f &= -(1+\xi_{\text{in}})p_0\frac{\varepsilon_9}{\bar{h}_0^2}\bar{q}_y\left(q_{y0} - \frac{\bar{q}_y}{\bar{h}_0}h_0\right) \quad \text{at } y = 0,\\
\varepsilon^2 f &= \xi_{\text{ex}}p_0\frac{\varepsilon_9}{\bar{h}_0^2}\bar{q}_y\left(q_{y0} - \frac{\bar{q}_y}{\bar{h}_0}h_0\right) \quad \text{at } y = 1,
\end{aligned} \tag{47}$$

where

$$p_0 = \pi\rho\frac{R_0^3}{\widetilde{H}M_0} \tag{48}$$

is a new nondimensional parameter (involving the factor $\rho L^2/M_0$ in (43), a π from the integration over x, and R_0 replacing L due to the use of ε).

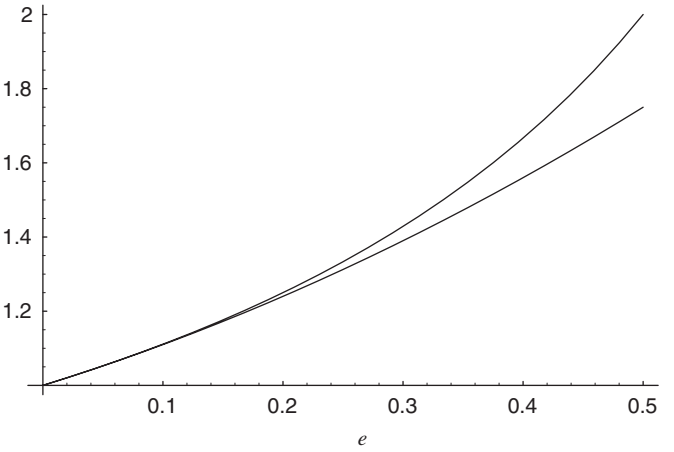

Fig. 2. Check on range of validity of (44). Upper curve: the function $1/(1-e)$. Lower curve: the Taylor approximation $1 + e + e^2$.

The functions $\varepsilon_1, \varepsilon_2, \ldots, \varepsilon_9$, listed in Appendix B, represent the offset. Without offset ($e = 0$), all of them are identically equal to 1.

6. Discretization

The Bubnov–Galerkin finite element method (Cook et al., 1989, Chapter 15; Zienkiewicz and Taylor, 1991, Chapters 11, 12) will be applied for discretizing and solving the coupled fluid and rod differential equations (33), (45), and (46), subject to the boundary conditions (34) and (47). The rod, and the fluid surrounding it, is divided into N_e finite elements of equal lengths, ℓ_e. Within each element e, the gap perturbation (and rod displacement) h_{0e}, the axial flow rate perturbation q_{y0e}, and the fluid force f_e are approximated as

$$h_{0e}(y,\tau) = \mathbf{N}(y)\mathbf{h}_e(\tau), \quad q_{y0e}(y,\tau) = \mathbf{N}(y)\mathbf{q}_e(\tau), \quad f_e(y,\tau) = \mathbf{N}(y)\mathbf{f}_e(\tau), \tag{49}$$

where $\mathbf{N}(y)$ is a row vector (matrix of dimension 1×4) of shape functions (cubic polynomials, see Appendix E) and $\mathbf{h}_e(\tau)$, $\mathbf{q}_e(\tau)$, and $\mathbf{p}_e(\tau)$ are column vectors (matrices of dimension 4×1) which represent generalized element nodal coordinates.

By (i) inserting (49) into (33), (45), and (46); (ii) multiplying these equations with $\mathbf{N}^{\mathrm{T}}$ from left, and integrating over y; (iii) implementing the boundary conditions (34) and (47) via integration by parts; and (iv) assembling the systems of N_e element matrices, the discrete fluid equations (45), (46) and the rod equation (34) can be written on matrix form as

$$\mathbf{M}_f\ddot{\mathbf{h}} + \mathbf{C}_{fh1}\dot{\mathbf{h}} + \mathbf{C}_{fq1}\dot{\mathbf{q}} + \mathbf{S}_{fq1}\mathbf{q} = -\mathbf{F}_{f1}\mathbf{f}, \tag{50}$$

$$\mathbf{C}_{fh2}\dot{\mathbf{h}} + \mathbf{C}_{fq2}\dot{\mathbf{q}} + \mathbf{S}_{fh2}\mathbf{h} + \mathbf{S}_{fq2}\mathbf{q} = -\mathbf{F}_{f2}\mathbf{f}, \tag{51}$$

$$\mathbf{M}_s\ddot{\mathbf{h}} + \mathbf{C}_s\dot{\mathbf{h}} + \mathbf{K}_s\mathbf{h} = \mathbf{F}_s\mathbf{f}, \tag{52}$$

where a dot means differentiation with respect to the nondimensional time variable τ. The vectors $\mathbf{h}$, $\mathbf{q}$, and $\mathbf{f}$ are, respectively, the global rod deflection vector, the axial flow rate perturbation vector, and the fluid force vector. The matrices denoted by $\mathbf{M}$ are mass matrices, those denoted by $\mathbf{C}$ are damping matrices, and those denoted by $\mathbf{S}$ are fluid loading matrices. Subscript 's' refers to 'solid' and subscript 'f' to fluid. Finally, $\mathbf{K}_s$ is the structural stiffness matrix, and the matrices denoted by $\mathbf{F}$ are fluid-structure coupling matrices. The structural matrices are all symmetric. The fluid equations however include asymmetric load, damping, and fluid-structure coupling matrices, which are responsible for the interesting dynamical behaviour of the system (see Sections 8 and 9).

The implementation of the fluid boundary conditions is shown in Appendix D. The element matrices are given in Appendix E. [For assembly of the element matrices into global matrices, and implementation of structural boundary conditions, we refer to Cook et al. (1989) and Zienkiewicz and Taylor (1991).]

By defining a state vector $\{\mathbf{h}\ \mathbf{q}\ \mathbf{f}\}^{\mathrm{T}}$ the coupled equations (50)–(52) can be grouped into a single matrix system on the form

$$\begin{bmatrix} \mathbf{M}_f & \mathbf{0} & \mathbf{0} \\ \mathbf{0} & \mathbf{0} & \mathbf{0} \\ \mathbf{M}_s & \mathbf{0} & \mathbf{0} \end{bmatrix} \begin{Bmatrix} \ddot{\mathbf{h}} \\ \ddot{\mathbf{q}} \\ \ddot{\mathbf{f}} \end{Bmatrix} + \begin{bmatrix} \mathbf{C}_{fh1} & \mathbf{C}_{fq1} & \mathbf{0} \\ \mathbf{C}_{fh2} & \mathbf{C}_{fq2} & \mathbf{0} \\ \mathbf{C}_s & \mathbf{0} & \mathbf{0} \end{bmatrix} \begin{Bmatrix} \dot{\mathbf{h}} \\ \dot{\mathbf{q}} \\ \dot{\mathbf{f}} \end{Bmatrix} + \begin{bmatrix} \mathbf{0} & \mathbf{S}_{fq1} & \mathbf{F}_{f1} \\ \mathbf{S}_{fh2} & \mathbf{S}_{fq2} & \mathbf{F}_{f2} \\ \mathbf{K}_s & \mathbf{0} & -\mathbf{F}_s \end{bmatrix} \begin{Bmatrix} \mathbf{h} \\ \mathbf{q} \\ \mathbf{f} \end{Bmatrix} = \{\mathbf{0}\}. \tag{53}$$

The matrices can, from left to right, be considered as a generalized mass, damping, and stiffness matrix, respectively.

7. Eigenvalue problem

The generalized mass matrix in (53) is singular,[1] so this matrix system cannot be directly brought into a standard, first-order system. To circumvent this problem, (52) is rewritten as

$$\mathbf{f} = \mathbf{F}_s^{-1}[\mathbf{M}_s\ddot{\mathbf{h}} + \mathbf{C}_s\dot{\mathbf{h}} + \mathbf{K}_s]. \tag{54}$$

[1]This appears to be typical in coupled problems, see e.g. Zienkiewicz and Taylor (1991, p. 422) and Lesoinne et al. (2001). The latter reference gives a different method for circumventing a similar though not identical problem; the former reference does not consider an eigenvalue analysis, but a transient analysis.

Inserting this into (50)–(51) gives two new coupled fluid-structure equations,

$$\mathbf{M}_a\ddot{\mathbf{h}} + \mathbf{C}_{ha}\dot{\mathbf{h}} + \mathbf{C}_{qa}\dot{\mathbf{q}} + \mathbf{S}_{ha}\mathbf{h} + \mathbf{S}_{qa}\mathbf{q} = \mathbf{0}, \tag{55}$$

$$\mathbf{M}_b\ddot{\mathbf{h}} + \mathbf{C}_{hb}\dot{\mathbf{h}} + \mathbf{C}_{qb}\dot{\mathbf{q}} + \mathbf{S}_{hb}\mathbf{h} + \mathbf{S}_{qb}\mathbf{q} = \mathbf{0}, \tag{56}$$

where $\mathbf{M}_a = \mathbf{M}_f + \mathbf{F}_{f1}\mathbf{F}_s^{-1}\mathbf{M}_s$, $\mathbf{C}_{ha} = \mathbf{C}_{fh1} + \mathbf{F}_{f1}\mathbf{F}_s^{-1}\mathbf{C}_s$, and equivalently for the remaining terms. [The force vector $\mathbf{f}$ could also have been isolated from (50), or (51).] By introducing the additional variable $\mathbf{v} = \dot{\mathbf{h}}$, (55)–(56) can be grouped into the first-order system

$$\begin{bmatrix} \mathbf{S}_{ha} & \mathbf{0} & \mathbf{S}_{qa} \\ \mathbf{S}_{hb} & \mathbf{0} & \mathbf{S}_{qb} \\ \mathbf{0} & -\mathbf{I} & \mathbf{0} \end{bmatrix} \begin{Bmatrix} \mathbf{h} \\ \mathbf{v} \\ \mathbf{q} \end{Bmatrix} = - \begin{bmatrix} \mathbf{C}_{ha} & \mathbf{M}_a & \mathbf{C}_{qa} \\ \mathbf{C}_{hb} & \mathbf{M}_b & \mathbf{C}_{qb} \\ \mathbf{I} & \mathbf{0} & \mathbf{0} \end{bmatrix} \begin{Bmatrix} \dot{\mathbf{h}} \\ \dot{\mathbf{v}} \\ \dot{\mathbf{q}} \end{Bmatrix}. \tag{57}$$

With discretization into N_e finite elements, the matrices in (57) will be of size[2] $6N_e \times 6N_e$. Setting $\{\mathbf{h}(\tau)\ \mathbf{v}(\tau)\ \mathbf{q}(\tau)\}^{\mathrm{T}} = \{\hat{\mathbf{h}}\ \hat{\mathbf{v}}\ \hat{\mathbf{q}}\}^{\mathrm{T}} \exp(\Lambda\tau)$, Eq. (57) has the standard form of the 'extended' eigenvalue problem $\mathbf{Az} = \Lambda\mathbf{Bz}$. This is solved using the QR method (Press et al., 1992).

The equilibrium configuration of the rod ($h(y,\tau) \equiv e$) is stable if all eigenvalues Λ_j satisfy $\mathrm{Re}(\Lambda_j) < 0$. The equilibrium configuration is unstable if $\mathrm{Re}(\Lambda_j) > 0$ for at least one j. The instability is of divergence (flutter) type if $\mathrm{Im}(\Lambda_j) = (\neq)0$. The flow speed $\bar{V}$ where instability is initiated will be referred to as the critical flow speed $\bar{V}_{cr}$.

8. Numerical results

Discussion of the stability characteristics (behaviour of eigenvalues) will be given in terms of physical (dimensional) parameters. Specifically, dimensional eigenvalues[3] $\bar{\Lambda} = \Lambda\tau_*$ [s^{-1}] will be shown as functions of the dimensional mean axial flow speed $\bar{V}$ [$\mathrm{m\,s}^{-1}$] defined by (20). Although the theory has been formulated in terms of nondimensional parameters, the use of dimensional parameters is thought to be more informative in the present context, and it makes direct comparison with the results given in earlier studies, e.g. (Fujita and Shintani, 2001; Fujita et al., 2004), possible. The eigenvalue projection to be used is similar to the one employed in Païdoussis et al. (1990).

Results will be presented for two different rod materials (PVC and silicone rubber) and two different fluids (water and air), following basically examples given in Fujita and Shintani (2001) and Fujita et al. (2004). In examples with hollow rods, the internal radius will be denoted by R_i. Rod material and fluid data are given in Tables 1 and 2. Pressure loss coefficients ξ_{in}, ξ_{ex} are both set equal to zero. Structural damping (Kelvin–Voigt type) is included, using the value $E^* = 2 \times 10^5\ \mathrm{N\,s\,m}^{-2}$ in any example (Sugiyama et al., 1985). It has been confirmed that inclusion of structural damping does not affect the predicted critical flow speeds to any significant extent. [Divergence instability boundaries are not affected by damping; only flutter instability boundaries.] Inclusion of Kelvin–Voigt type damping is, however, convenient from a numerical point of view, because it effectively and realistically damps the higher modes with higher intensity (Bishop and Fawzy, 1976).

8.1. Influence of flow model

Figs. 3 and 4 show the real and imaginary components of the eigenvalues as function of the mean flow speed for a hollow, simply supported PVC-rod in water flow. [Only the positive branches of $\mathrm{Im}(\bar{\Lambda})$ are shown. It is also to be noted that the curves have been plotted with dots (i.e., not with lines) due to their complexity. This is the reason for the 'dotted line appearance' in places with large gradients.] The dimensions of the rod are as follows: $R_0 = 10\,\mathrm{mm}$, $R_i = 7\,\mathrm{mm}$, and $L = 1000\,\mathrm{mm}$. The fluid gap varies from 5 mm down to 1 mm, as indicated in the figure captions. Laminar flow is assumed in Fig. 3, while the correct (laminar-turbulent) friction model is used in Fig. 4.

To any eigenvalue $\bar{\Lambda}$ there is an eigenvector $\mathbf{z}^{\mathrm{T}} = \{\hat{\mathbf{h}}\ \hat{\mathbf{v}}\ \hat{\mathbf{q}}\}^{\mathrm{T}}$ which includes both the structural variables $\hat{\mathbf{h}}$ and $\hat{\mathbf{v}}$, and the fluid variables $\hat{\mathbf{q}}$, see Eq. (57). Each eigenvalue branch is thus related to a 'mode' of the coupled fluid-structure system. There are no pure 'fluid modes' and no pure 'solid modes' (Barbone and Crighton, 1994). The almost linear, 'fan-like' eigenvalue branches are, however, due to inclusion of $\hat{\mathbf{q}}$ in the eigenvalue problem. They are not present in a formulation based on a relation like (42), where the flow rate perturbation has been eliminated. [Compare, for example, with the eigenvalue curves in Païdoussis et al. (1990) and Fujita and Shintani (2001).]

[2]Each node has two degrees of freedom (Cook et al., 1989).

[3]For τ_* and Λ, see Eq. (27) and the text following Eq. (57), respectively.

Table 1
Rod data

Material	Density ρ_r (kg m^{-3})	Young's modulus E (N m^{-2})
PVC	1.40×10^3	3.00×10^9
Silicone rubber	1.20×10^3	9.44×10^7

Table 2
Fluid data

Fluid	Density ρ (kg m^{-3})	Kinematic viscosity ν (m^2 s^{-1})
Water	998	1.004×10^{-6}
Air	1.205	1.500×10^{-5}

The 'linear' eigenvalue branches are predominantly related to fluid motion, while the 'remaining' branches are predominantly related to structural motion (although they are, of course, strongly modified by the fluid flow). Then, inspired by Chen and Rosenberg (1975), we will refer to the former as 'fluid branches', and to the latter as 'solid branches' (to have a convenient means of reference).

That the fluid branches are (almost) linear can be understood by imagining a fluid flow past a completely rigid rod. Then the structural deflection $\hat{\mathbf{h}}$ will not appear in (50) and (51), which can be reduced to a single matrix equation (eigenvalue problem) of the form $\bar{\Lambda}\mathbf{U}\hat{\mathbf{q}} = \mathbf{V}\hat{\mathbf{q}}$. By inspection of (E.1) and (E.2) in Appendix E (or of (45) and (46)) it can be seen that $\mathbf{U}$ will be independent of the mean flow rate q_{y0}, while $\mathbf{V}$ will depend linearly on it. Accordingly, any eigenvalue $\bar{\Lambda}$ will be a linear function of the mean flow speed $\bar{V}$.

The critical flow speeds related to Figs. 3 and 4 are summarized in Table 3. The corresponding critical Reynolds numbers $\mathrm{Re}_{cr} = \bar{V}_{cr}\bar{H}_0/\nu$ are also included. The results are obtained using ten finite elements ($N_e = 10$). Table 4 indicates that this gives the critical flow speed to three significant figures (while clamped boundary conditions are somewhat more demanding). Accordingly, any result for simply supported rods in this section is obtained with $N_e = 10$, unless stated otherwise.

A divergence instability is initiated in any of the 10 cases shown in Figs. 3 and 4. The instability originates from coalescence of a pair of complex conjugate eigenvalues on the $\mathrm{Im}(\bar{\Lambda}) = 0$ axis (i.e., a pitchfork bifurcation), at the speed $\bar{V}_{pb}$, say. But the corresponding real parts are less than zero, so instability is not initiated immediately. This happens at a slightly higher flow speed, $\bar{V}_{cr}$, where the uppermost branch crosses the line $\mathrm{Re}(\bar{\Lambda}) = 0$.

By comparing the results for corresponding fluid gaps in Figs. 3 and 4 it will be seen that the bifurcation point speeds $\bar{V}_{pb}$ in general are lower for the turbulent model. Values of the critical speeds $\bar{V}_{cr}$ are, however, about the same (see again Table 3).

It is interesting to note that by the turbulent model the 'divergence bubble' moves further and further down by decreasing fluid gap. For $\bar{H}_0 = 1$ mm it has moved below the $\mathrm{Re}(\bar{\Lambda}) = 0$ line, resulting in a significant increase in $\bar{V}_{cr}$. [Flutter, rather than divergence, is initiated at $\bar{V}_{cr} = 53.9\,\mathrm{m\,s^{-1}}$ ($\mathrm{Re}_{cr} = 53.7 \times 10^3$). More examples on flutter will follow a little later in this subsection.]

Figs. 5 and 6 are for a massive, simply supported silicone rubber rod in water and air flow, respectively. The rod length $L = 800$ mm, the radius $R_0 = 8$ mm, and the fluid gap $\bar{H}_0 = 4$ mm (corresponding to the case considered by Fujita et al., 2004, both theoretically and experimentally). Parts (a) are obtained with the laminar flow model, while parts (b) are obtained with the turbulent flow model. With water flow (Fig. 5(a)) the laminar model gives the critical flow speed $\bar{V}_{cr} = 3.43\,\mathrm{m\,s^{-1}}$ ($\mathrm{Re}_{cr} = 13.6 \times 10^3$), while $\bar{V}_{cr} = 3.38\,\mathrm{m\,s^{-1}}$ ($\mathrm{Re}_{cr} = 13.4 \times 10^3$) is obtained with the turbulent model (Fig. 5(b)). With air flow (Fig. 6) the values are $\bar{V}_{cr} = 98.4\,\mathrm{m\,s^{-1}}$ ($\mathrm{Re}_{cr} = 26.2 \times 10^3$) for the laminar

Fig. 3. Real and imaginary parts of the eigenvalues $\bar{\Lambda}[\mathrm{s^{-1}}]$ as functions of the flow speed $\bar{V}[\mathrm{m\,s^{-1}}]$, for a simply supported (pinned–pinned) rod in various fluid gaps $\bar{H}_0$, using a *laminar flow* model. [Rod material: PVC; dimensions: $L = 1000$ mm, $R_0 = 10$ mm, $R_i = 7$ mm; fluid: water.] (a) $\bar{H}_0 = 5$ mm: $\bar{V}_{cr} = 16.80\,\mathrm{m\,s^{-1}}$ ($\mathrm{Re}_{cr} = 83.7 \times 10^3$); (b) $\bar{H}_0 = 4$ mm: $\bar{V}_{cr} = 15.05\,\mathrm{m\,s^{-1}}$ ($\mathrm{Re}_{cr} = 60.0 \times 10^3$); (c) $\bar{H}_0 = 3$ mm: $\bar{V}_{cr} = 13.05\,\mathrm{m\,s^{-1}}$ ($\mathrm{Re}_{cr} = 39.0 \times 10^3$); (d) $\bar{H}_0 = 2$ mm: $\bar{V}_{cr} = 10.65\,\mathrm{m\,s^{-1}}$ ($\mathrm{Re}_{cr} = 21.2 \times 10^3$); (e) $\bar{H}_0 = 1$ mm: $\bar{V}_{cr} = 8.15\,\mathrm{m\,s^{-1}}$ ($\mathrm{Re}_{cr} = 8.11 \times 10^3$).

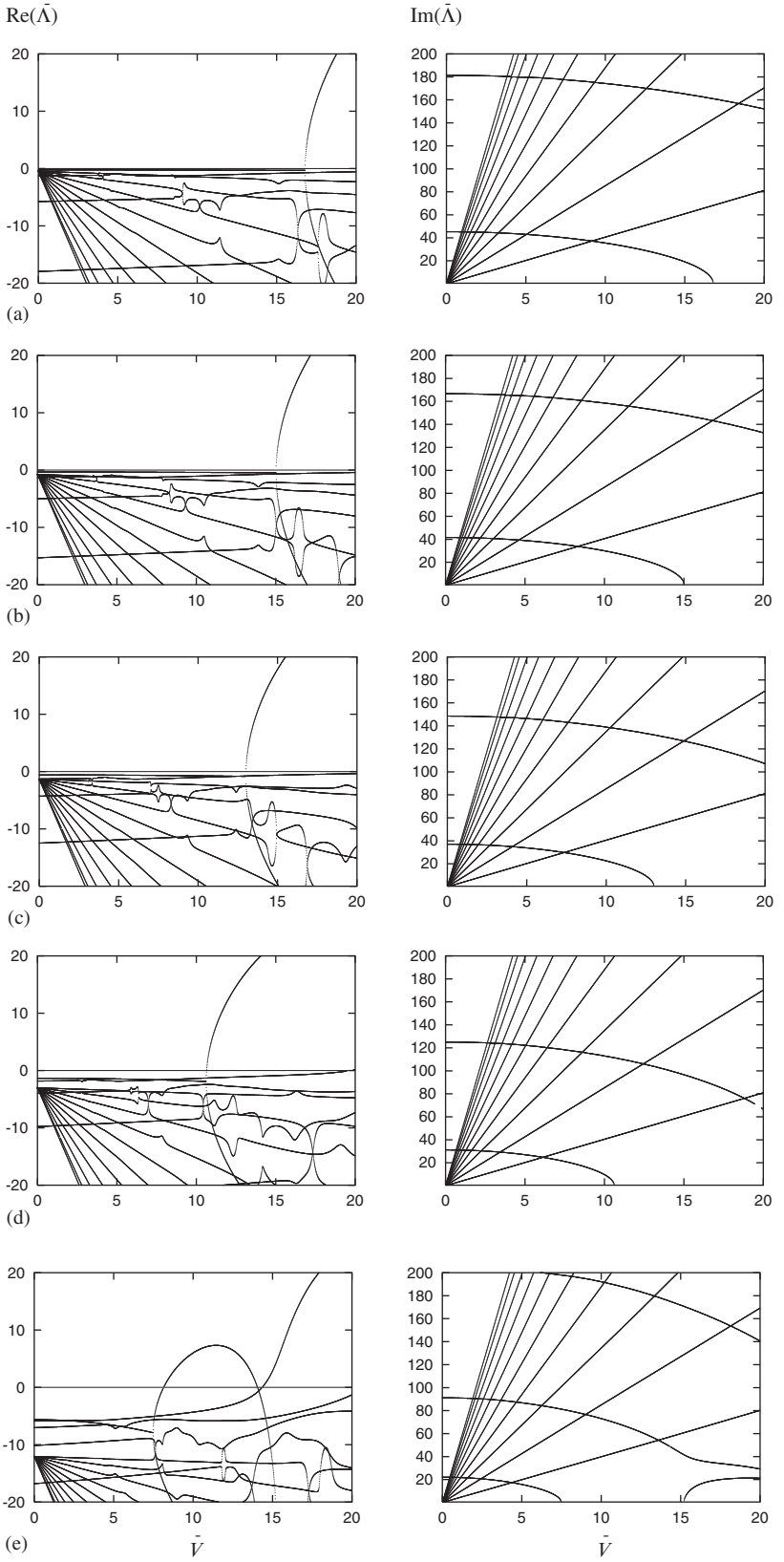
Re($\bar{\Lambda}$)
Im($\bar{\Lambda}$)
(a)
(b)
(c)
(d)
(e)
$\bar{V}$
$\bar{V}$

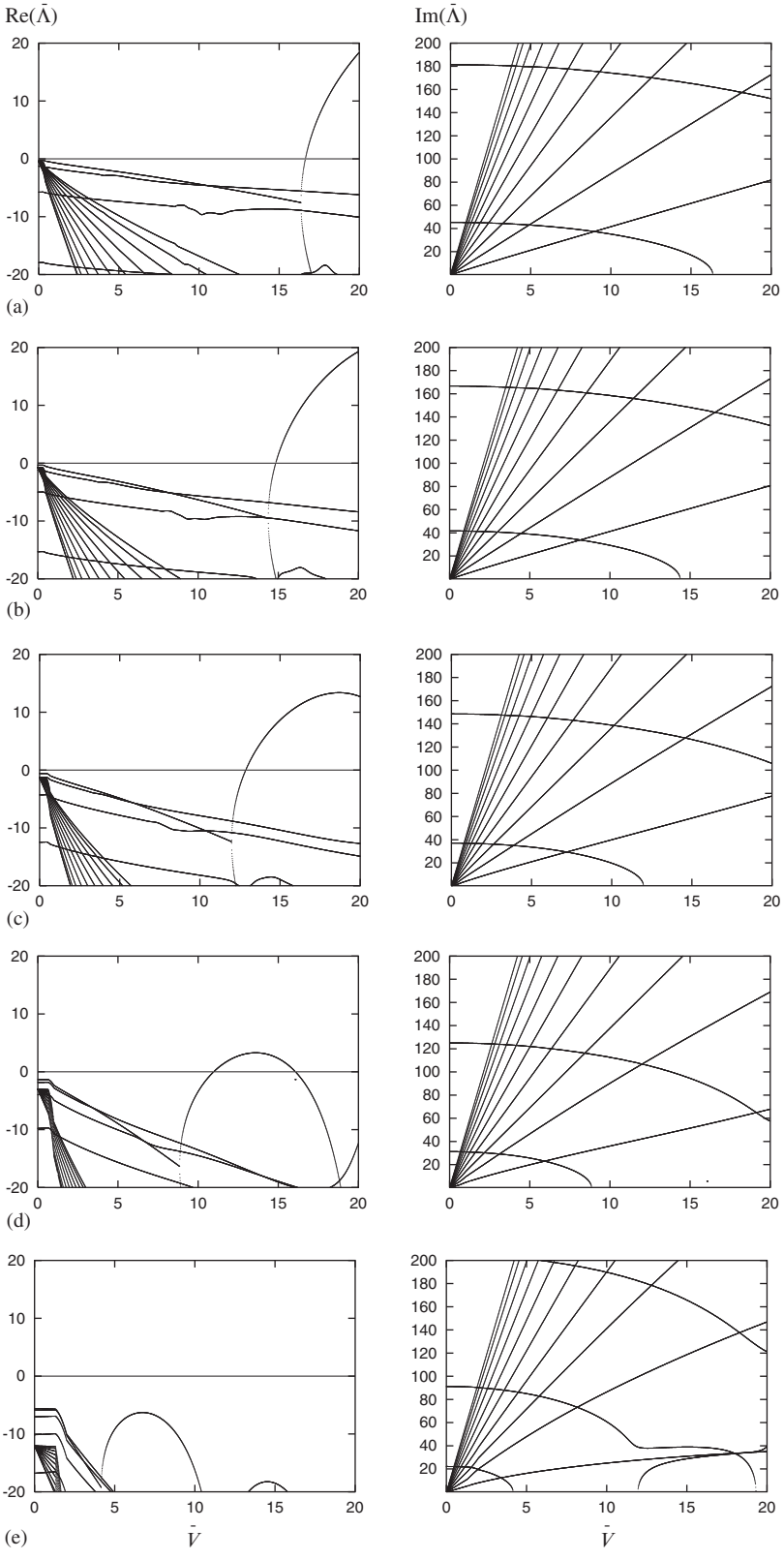
Re($\bar{\Lambda}$)
Im($\bar{\Lambda}$)
(a)
(b)
(c)
(d)
(e)
$\bar{V}$
$\bar{V}$

Table 3
Influence of fluid gap $\bar{H}_0$ on the critical flow speed $\bar{V}_{cr}$ for a simply supported PVC rod in water flow. The rod dimensions are as follows: $L = 1000\,\text{mm}$, $R_0 = 10\,\text{mm}$, $R_i = 7\,\text{mm}$

Fluid gap $\bar{H}_0$ (mm)	$\bar{V}_{cr}$ lam. flow	Re_{cr} lam. flow	$\bar{V}_{cr}$ turb. flow	Re_{cr} turb. flow
5	16.80	83.7×10^3	16.65	82.9×10^3
4	15.05	60.0×10^3	14.85	59.2×10^3
3	13.05	39.0×10^3	12.90	38.5×10^3
2	10.65	21.2×10^3	10.98	21.9×10^3
1	8.15	8.12×10^3	53.9 (flutter)	53.7×10^3

Table 4
Influence of the number of finite elements N_e on the critical flow speed $\bar{V}_{cr}$ (m s^{-1}), for two different boundary conditions

N_e	10	20	30	40	50	60
Clamped–clamped, $\bar{H}_0 = 4\,\text{mm}$	30.87	30.97	30.99	30.99	30.99	30.99
Pinned–pinned, $\bar{H}_0 = 2\,\text{mm}$	10.98	11.00	11.00	11.00	11.00	11.00

model and $\bar{V}_{cr} = 97.2\,\text{m s}^{-1}$ ($\text{Re}_{cr} = 25.9 \times 10^3$) for the turbulent model—again just a small difference. It is finally noted that the experiment performed by Fujita et al. (2004) gave the critical flow speed $\bar{V}_{cr} = 86\,\text{m s}^{-1}$, while their analysis, based on Galerkin's method, gives $\bar{V}_{cr} = 96\,\text{m s}^{-1}$.

The eigenvalue curves shown in Fig. 7 are for a hollow, simply supported silicone rubber rod in air flow. Again Fig. 7(a) is obtained with the laminar flow model and Fig. 7(b) with the turbulent model. The dimensions of the rod are as in the first example, that is, $R_0 = 10$, $R_i = 7$, $L = 1000\,\text{mm}$, and the fluid gap $\bar{H}_0 = 1\,\text{mm}$. In this case flutter is initiated at $\bar{V}_{cr}$. For the laminar flow model (Fig. 7(a)) the critical flow speed $\bar{V}_{cr} = 54.2\,\text{m s}^{-1}$ ($\text{Re}_{cr} = 3.61 \times 10^3$); for the turbulent model (Fig. 7(b)), $\bar{V}_{cr} = 45.4\,\text{m s}^{-1}$ ($\text{Re}_{cr} = 3.03 \times 10^3$). The corresponding flutter frequencies $\Omega_{cr} = \text{Im}(\bar{\lambda})_{cr}$ are 35.50 Hz and 38.50 Hz, respectively. [Increasing the number of finite elements to $N_e = 20$ does not alter the critical flow speeds nor the flutter frequencies to within three significant digits.]

Flutter of a simply supported rod by laminar flow ($\text{Re} < 2000$) is also possible. An example on this is obtained by increasing the length of the rod from the previous example to $L = 2000\,\text{mm}$; otherwise the data are the same. The eigenvalue curves are shown in Fig. 8. Flutter is initiated at $\bar{V}_{cr} = 11.80\,\text{m s}^{-1}$ ($\text{Re}_{cr} = 787$). The corresponding flutter frequency $\Omega_{cr} = 13.46\,\text{Hz}$. Also here, increasing the number of finite elements to $N_e = 20$ does not alter the critical flow speed nor the flutter frequency (to within three significant digits). Part (a) shows the 10-element solution, part (b) the 20-element solution. Fig. 9 shows the flutter oscillations (part a) and corresponding phase angle (part b), using $N_e = 20$. These figures will be discussed in the Section 9.

In the last example of this section we return to the case considered in Fig. 5, but replace the pinned–pinned boundary conditions by clamped-free conditions (a cantilever, clamped at the upstream end and free at the downstream end). The eigenvalue curves are shown in Fig. 10. Again, Fig. 10(a) is for the laminar model, while Fig. 10(b) is for the turbulent model. Both give a flutter instability at $\bar{V}_{cr}$; the laminar model gives $\bar{V}_{cr} = 11.50\,\text{m s}^{-1}$ ($\text{Re}_{cr} = 45.8 \times 10^3$) and $\Omega_{cr} = 30.26\,\text{Hz}$, while the turbulent model gives $\bar{V}_{cr} = 14.95\,\text{m s}^{-1}$ ($\text{Re}_{cr} = 59.6 \times 10^3$) and $\Omega_{cr} = 77.78\,\text{Hz}$ [$N_e = 10$ has been used here]. Fujita and Shintani (2001) report a similar example. The flutter instability is not surprising, because the jet discharging from the free end of the rod corresponds to a follower force, just as in the case of a cantilevered fluid-conveying pipe (Païdoussis, 1998). [This can be verified mathematically from (59), to be given in Section 9.]

It is finally noted that the complicated appearance of the eigenvalue branches in Fig. 10 is partly due to interactions between them: at a certain flow speed, one branch (branch A say) and its complex conjugate (which is not shown) collide with another pair of complex conjugate branches (branches B say); after the collision (i.e., at a slightly higher flow speed) the two pairs of branches change roles, such that branches A continue in the form of branches B, and vice versa. Interactions take place both between 'fluid modes' and 'solid modes', and between different 'solid modes'. A case

Fig. 4. Same as Fig. 3, but using the *turbulent flow* model. (a) $\bar{H}_0 = 5\,\text{mm}$: $\bar{V}_{cr} = 16.65\,\text{m s}^{-1}$ ($\text{Re}_{cr} = 82.9 \times 10^3$); (b) $\bar{H}_0 = 4\,\text{mm}$: $\bar{V}_{cr} = 14.85\,\text{m s}^{-1}$ ($\text{Re}_{cr} = 59.2 \times 10^3$); (c) $\bar{H}_0 = 3\,\text{mm}$: $\bar{V}_{cr} = 12.90\,\text{m s}^{-1}$ ($\text{Re}_{cr} = 38.5 \times 10^3$); (d) $\bar{H}_0 = 2\,\text{mm}$: $\bar{V}_{cr} = 10.98\,\text{m s}^{-1}$ ($\text{Re}_{cr} = 21.9 \times 10^3$); (e) $\bar{H}_0 = 1\,\text{mm}$: $\bar{V}_{cr} = 59.3\,\text{m s}^{-1}$ ($\text{Re}_{cr} = 53.7 \times 10^3$) (flutter instability).

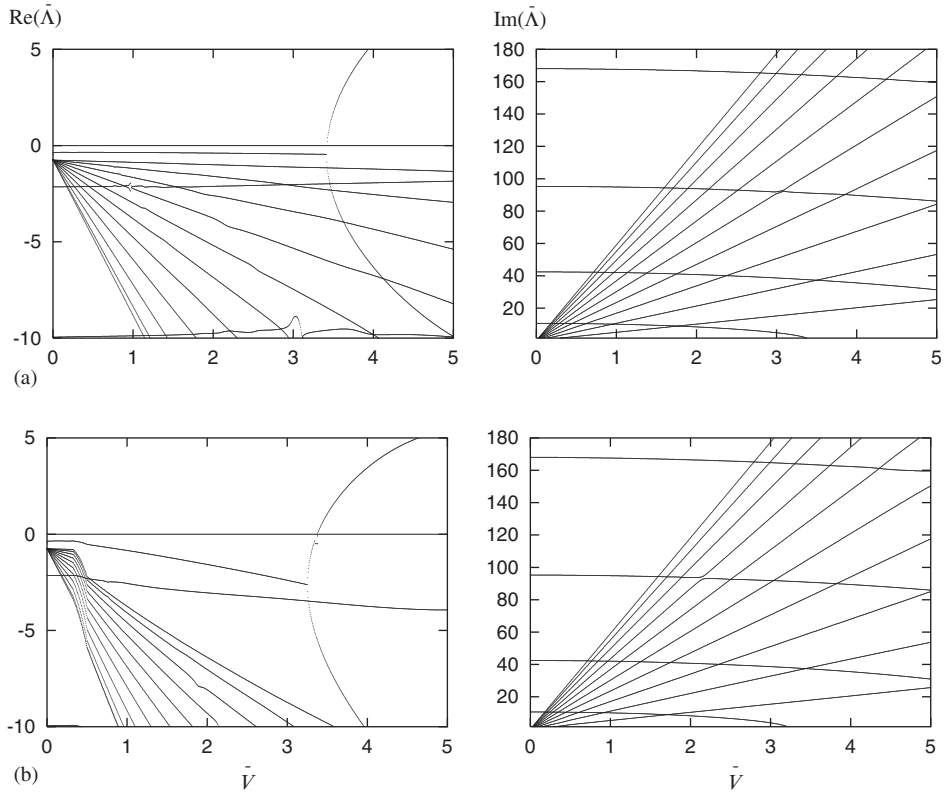

Fig. 5. Influence of flow model (laminar/turbulent) on real and imaginary parts of the eigenvalues, for a simply supported (pinned–pinned) rod in a $\bar{H}_0 = 4$ mm fluid gap. [Rod material: silicone rubber; dimensions: $L = 800$ mm, $R_0 = 8$ mm, $R_i = 0$ mm; fluid: water.] (a) Laminar flow: $\bar{V}_{cr} = 3.425\,\mathrm{m\,s^{-1}}$ ($\mathrm{Re}_{cr} = 13.6 \times 10^3$); (b) turbulent flow: $\bar{V}_{cr} = 3.375\,\mathrm{m\,s^{-1}}$ ($\mathrm{Re}_{cr} = 13.4 \times 10^3$).

of interaction between 'fluid modes' and 'solid modes' is also apparent in Fig. 5 (see the imaginary parts). [The phenomenon is also seen in the dynamics of fluid-conveying pipes (Bishop and Fawzy, 1976; Païdoussis, 1998), fluid-conveying shells (Chen and Rosenberg, 1975; Païdoussis, 2004), and Beck's column with damping (Langthjem, 1994).]

8.2. *Influence of equilibrium offset*

The influence of equilibrium offset is illustrated by Table 5. Case I is related to the divergence example of Fig. 5 and Case II to the flutter example of Fig. 8. It is found that offset lowers the critical flow speed for both divergence and flutter. This seems plausible as the offset 'scales up' the fluid matrices (see Appendices D and E) and thus the fluid loading, while the stiffness of the rod remains the same. Li et al. (2002) observed a similar effect in the case of a spring-mounted rigid rod.

9. Mechanism of instability

This section attempts to explain the possible mechanisms behind the divergence and flutter instabilities, and why the critical flow speed is largely insensitive to the flow model (laminar or turbulent) by divergence but quite sensitive to it by flutter.

The analysis is made under the assumptions of laminar flow and zero equilibrium offset, such that the displacement–pressure relation (42) can be used.

By integrating the pressure over the rod surface, as explained in Section 5, a displacement-fluid force relation is obtained as

$$\varepsilon^2 \frac{\partial^2 f}{\partial y^2} - f = p_0 \left[\frac{1}{\bar{h}} \frac{\partial^2 h_0}{\partial \tau^2} + \frac{2\bar{q}_y}{\bar{h}^2} \frac{\partial^2 h_0}{\partial y \partial \tau} + \frac{\beta}{\bar{h}^3} \frac{\partial h_0}{\partial \tau} + \beta \frac{3\bar{q}_y}{\bar{h}^4} \frac{\partial h_0}{\partial y} + \frac{1}{\bar{h}^3} \frac{\partial^2 h_0}{\partial y^2} \right]. \tag{58}$$

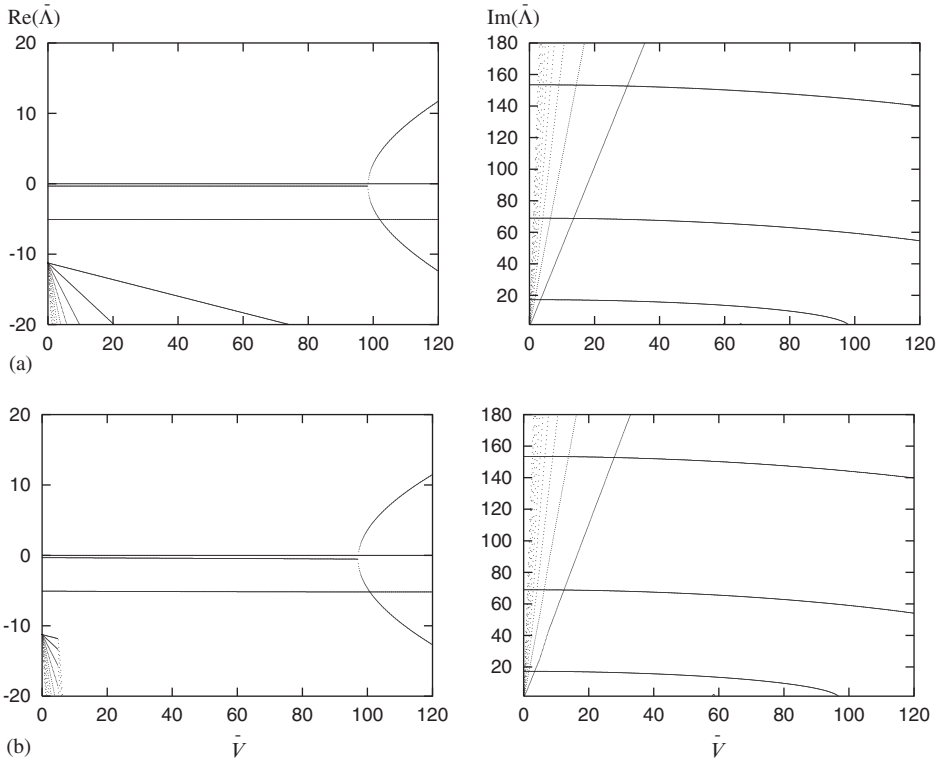

Fig. 6. Same as Fig. 5, but with air (instead of water). (a) Laminar flow: $\bar{V}_{cr} = 98.40\,\mathrm{m\,s^{-1}}$ ($\mathrm{Re}_{cr} = 26.2 \times 10^3$); (b) turbulent flow: $\bar{V}_{cr} = 97.20\,\mathrm{m\,s^{-1}}$ ($\mathrm{Re}_{cr} = 25.9 \times 10^3$).

This equation can be coupled with (33) to give the single fluid-structure force balance equation

$$\frac{\partial^2}{\partial\tau^2}\left\{\left(m+\frac{p_0}{\bar{h}_0}\right)h_0-\varepsilon^2 m\,\frac{\partial^2 h_0}{\partial y^2}\right\}+\frac{\partial}{\partial\tau}\left\{c\left(\frac{\partial^4 h_0}{\partial y^4}-\varepsilon^2\,\frac{\partial^6 h_0}{\partial y^6}\right)+p_0\left(2\,\frac{\bar{q}_y}{\bar{h}_0^2}\,\frac{\partial h_0}{\partial y}+\frac{\beta}{\bar{h}_0^3}\,h_0\right)\right\}$$
$$+k\left\{\frac{\partial^4 h_0}{\partial y^4}-\varepsilon^2\,\frac{\partial^6 h_0}{\partial y^6}\right\}+p_0\left(3\beta\,\frac{\bar{q}_y}{\bar{h}_0^4}\,\frac{\partial h_0}{\partial y}+\frac{\bar{q}_y^2}{\bar{h}_0^3}\,\frac{\partial^2 h_0}{\partial y^2}\right)=0, \tag{59}$$

valid under the conditions stated in Section 4.3. This must be emphasized because it implies, among other things but most importantly, that the fluid boundary conditions (32) *must* be in the form $p = 0$ at $y = 0, 1$—a condition satisfied only with, at least, simply supported rod ends. Accordingly, *only pinned–pinned and clamped–clamped boundary conditions will be considered in the following*.

As $\varepsilon^2 \ll 1$ in all the numerical examples considered, the terms in (59) multiplied by this factor may be neglected. We will, however, for completeness, keep these terms in the discussion to follow.

9.1. Divergence

Divergence is independent of time. Removing the explicitly time-dependent terms from (59) gives the static force balance equation

$$k\left\{\frac{\partial^4 h_0}{\partial y^4}-\varepsilon^2\,\frac{\partial^6 h_0}{\partial y^6}\right\}+p_0\left[3\beta\,\frac{\bar{q}_y}{\bar{h}_0^4}\,\frac{\partial h_0}{\partial y}+\frac{\bar{q}_y^2}{\bar{h}_0^3}\,\frac{\partial^2 h_0}{\partial y^2}\right]=0. \tag{60}$$

Here the terms in curly brackets {} make up the flexural restoring force. The first term in square brackets [] is a (tangential and thus nonconservative) fluid friction force. The second term in square brackets is a 'centrifugal force' due to the moving load provided by the flowing fluid; it corresponds to the compressive end load in the usual Euler buckling problem. This term originates from the convective term $\partial(Q_Y^2/H)/\partial Y$ in (2).

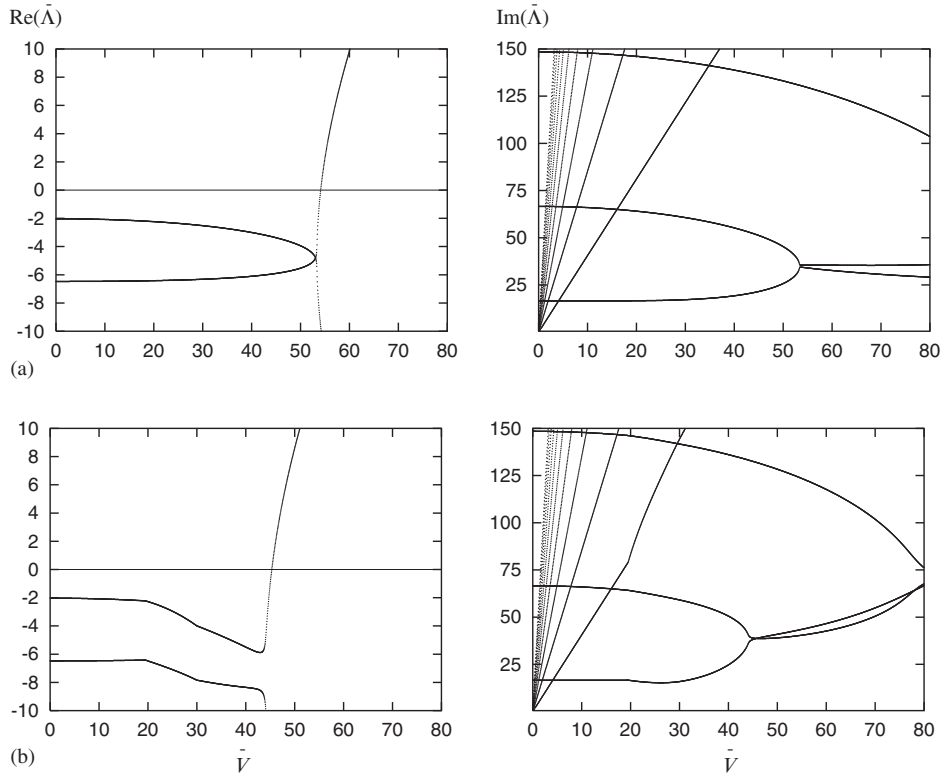

Fig. 7. Real and imaginary parts of the eigenvalues $\bar{\Lambda}[\mathrm{s}^{-1}]$ as functions of the flow speed $\bar{V}[\mathrm{m\,s}^{-1}]$, for a simply supported (pinned–pinned) rod in air flow. [Rod material: silicone rubber; dimensions: $L = 1000\,\mathrm{mm}$, $R_0 = 10\,\mathrm{mm}$, $R_i = 7\,\mathrm{mm}$, $\bar{H}_0 = 1\,\mathrm{mm}$]. (a) Laminar flow model: $\bar{V}_{cr} = 54.20\,\mathrm{m\,s}^{-1}$ ($\mathrm{Re}_{cr} = 3613$), $\Omega_{cr} = 35.50\,\mathrm{Hz}$; (b) turbulent flow model: $\bar{V}_{cr} = 45.40\,\mathrm{m\,s}^{-1}$ ($\mathrm{Re}_{cr} = 3027$), $\Omega_{cr} = 38.50\,\mathrm{Hz}$.

It can be shown that the fluid friction force does not affect the divergence flow speed if the boundary conditions satisfy the equation[4] $h_0(0) = h_0(1)$. This will be done by consideration of a work-energy balance equation, obtained by multiplying (60) by the rod deflection h_0, followed by integration along the rod, $0 \leqslant y \leqslant 1$.

Considering first the friction term $p_0 3\beta(\bar{q}_y/\bar{h}_0^4)(\partial h_0/\partial y)$, integration by parts gives (leaving out the factor $p_0 3\beta\bar{q}_y/\bar{h}_0^4$)

$$\int_0^1 h_0 \frac{\partial h_0}{\partial y}\,\mathrm{d}y = \frac{1}{2}\left[h_0^2\right]_0^1. \tag{61}$$

Thus, if $h_0(0) = h_0(1)$, as it is by clamped–clamped and pinned–pinned rod ends, we have

$$\int_0^1 h_0 \frac{\partial h_0}{\partial y}\,\mathrm{d}y = 0. \tag{62}$$

The remaining terms are

$$k\,\frac{1}{2}\left\{\int_0^1 \left(\frac{\partial^2 h_0}{\partial y^2}\right)^2 \mathrm{d}y + \varepsilon^2 \int_0^1 \left(\frac{\partial^3 h_0}{\partial y^3}\right)^2 \mathrm{d}y\right\} - p_0\,\frac{\bar{q}_y^2}{\bar{h}_0^3}\,\frac{1}{2}\int_0^1 \left(\frac{\partial h_0}{\partial y}\right)^2 \mathrm{d}y = 0. \tag{63}$$

This equation shows that the 'centrifugal force' (the last term) is solely responsible for the divergence instability in the clamped–clamped and pinned–pinned cases. In other words, the onset of divergence is independent of fluid friction. It must be emphasized that this is under the conditions stated in Section 4.3, which make (59) valid. Turbulent flow (and equilibrium offset) may modify this conclusion. But it appears to support and explain the numerical results that inclusion of correct turbulent fluid friction (instead of laminar friction) only affects the predicted divergence speeds slightly.

[4]The time-dependence is suppressed in this subsection.

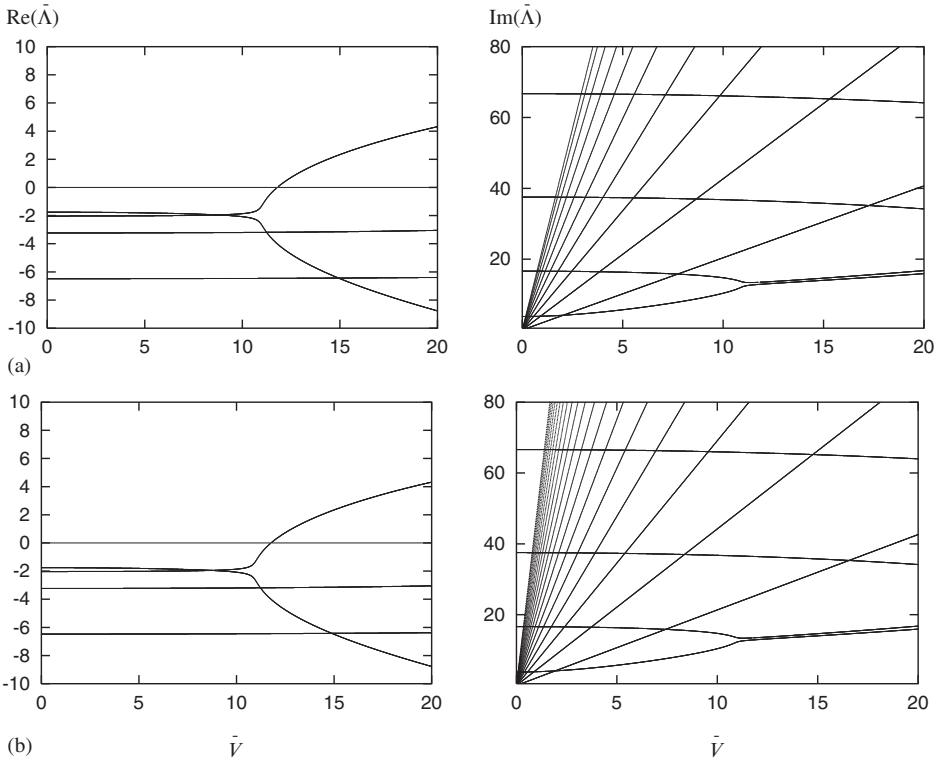

Fig. 8. Real and imaginary parts of the eigenvalues $\bar{\Lambda}[\mathrm{s}^{-1}]$ as functions of the flow speed $\bar{V}[\mathrm{m\,s}^{-1}]$, for a simply supported (pinned–pinned) rod in air flow. [Rod material: silicone rubber; dimensions: $L = 2000\,\mathrm{mm}$, $R_0 = 10\,\mathrm{mm}$, $R_i = 7\,\mathrm{mm}$, $\bar{H}_0 = 1\,\mathrm{mm}$]. (a) With 10 finite elements: $\bar{V}_{cr} = 11.80\,\mathrm{m\,s}^{-1}$ ($\mathrm{Re}_{cr} = 787$), $\Omega_{cr} = 13.46\,\mathrm{Hz}$; (b) with 20 finite elements: $\bar{V}_{cr} = 11.80\,\mathrm{m\,s}^{-1}$ ($\mathrm{Re}_{cr} = 787$), $\Omega_{cr} = 13.45\,\mathrm{Hz}$.

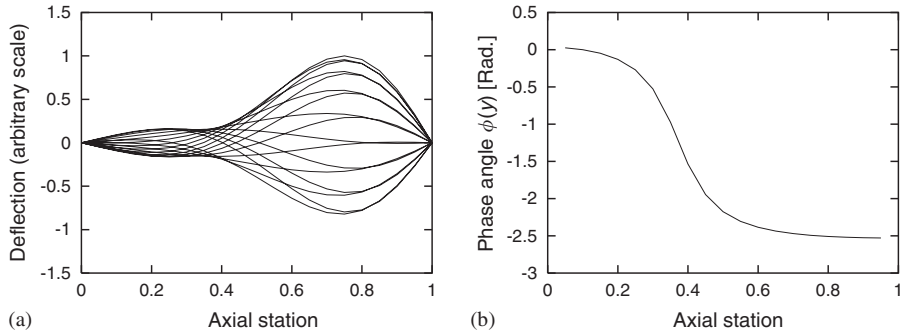

Fig. 9. (a) Flutter oscillations (at the onset of instability) for the case of Fig. 8; (b) corresponding phase angle.

9.2. *Flutter*

For the analysis of flutter, much information can be obtained from a power balance equation. As flutter is a dynamic instability, the start point must be the full version of (59). Multiplying this equation by the rod velocity $\partial h_0/\partial\tau$, followed by integration along the rod ($0 \leqslant y \leqslant 1$), gives the power balance equation

$$\frac{\partial}{\partial\tau}(\mathscr{T} + \mathscr{V}_i + \mathscr{V}_e) = -\mathscr{D}_{\mathrm{str}} - \mathscr{D}_{\mathrm{flu}} - \mathscr{P}_{nc}. \tag{64}$$

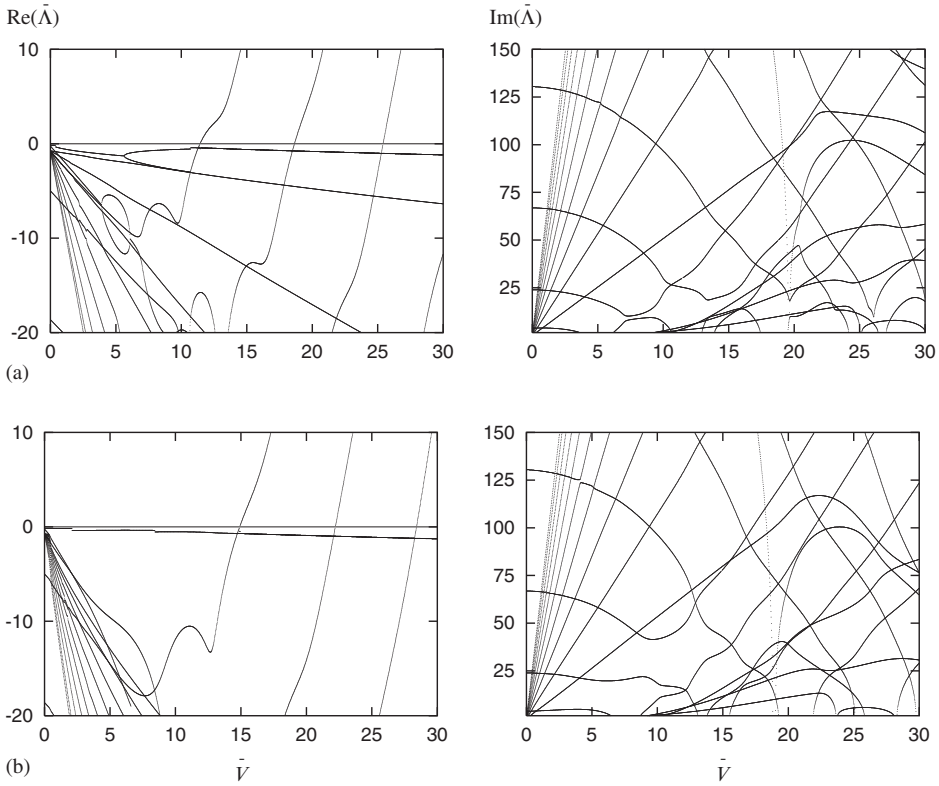

Fig. 10. Eigenvalue curves for the case of Fig. 5 but with clamped-free boundary conditions, rather than pinned–pinned. (a) Laminar flow model: $\bar{V}_{cr} = 11.50\,\mathrm{m\,s^{-1}}$ ($\mathrm{Re}_{cr} = 45.8 \times 10^3$), $\Omega_{cr} = 30.26\,\mathrm{Hz}$; (b) turbulent flow model: $\bar{V}_{cr} = 14.95\,\mathrm{m\,s^{-1}}$ ($\mathrm{Re}_{cr} = 59.6 \times 10^3$), $\Omega_{cr} = 77.78\,\mathrm{Hz}$.

Table 5
Influence of equilibrium offset on the critical flow speed $\bar{V}_{cr}$ ($\mathrm{m\,s^{-1}}$), for two different cases

$\mathscr{E}$	0	$0.1 \times \bar{H}_0$	$0.2 \times \bar{H}_0$	$0.3 \times \bar{H}_0$
Case I, $\bar{V}_{cr}$	3.38	3.33	3.19	3.03
Case II, $\bar{V}_{cr}$	11.80	11.34	11.00	10.30
Case II, Ω_{cr}	13.46	13.50	13.90	14.38

Case I: simply supported, massive silicone rubber tube, $L = 800\,\mathrm{mm}$, $R_0 = 8\,\mathrm{mm}$, $\bar{H}_0 = 4\,\mathrm{mm}$, with water flow. Case II: simply supported, hollow silicone rubber tube, $L = 2000\,\mathrm{mm}$, $R_0 = 10\,\mathrm{mm}$, $R_i = 7\,\mathrm{mm}$, $\bar{H}_0 = 1\,\mathrm{mm}$, in air flow.

Here

$$\mathscr{T} = \left(m + \frac{p_0}{\bar{h}_0}\right)\frac{1}{2}\int_0^1 \left(\frac{\partial h_0}{\partial \tau}\right)^2 \mathrm{d}y + \varepsilon^2 m \frac{1}{2}\int_0^1 \left(\frac{\partial^2 h_0}{\partial \tau \partial y}\right)^2 \mathrm{d}y \tag{65}$$

is the kinetic energy of the rod and the surrounding fluid,

$$\mathscr{V}_i = k\frac{1}{2}\left\{\int_0^1 \left(\frac{\partial^2 h_0}{\partial y^2}\right)^2 \mathrm{d}y + \varepsilon^2 \int_0^1 \left(\frac{\partial^3 h_0}{\partial y^3}\right)^2 \mathrm{d}y\right\} \tag{66}$$

is the elastic (bending) energy of the rod (internal potential energy),

$$\mathscr{V}_e = -p_0 \frac{\bar{q}_y^2}{\bar{h}_0^3}\frac{1}{2}\int_0^1 \left(\frac{\partial h_0}{\partial y}\right)^2 \mathrm{d}y \tag{67}$$

is the work done by conservative compressive forces (external potential energy),

$$\mathscr{D}_{\mathrm{str}} = c\left\{\int_0^1 \left(\frac{\partial^3 h_0}{\partial\tau\partial y^2}\right)^2 \mathrm{d}y + \varepsilon^2 \int_0^1 \left(\frac{\partial^4 h_0}{\partial\tau\partial y^3}\right)^2 \mathrm{d}y\right\} \tag{68}$$

is the rate of work done by structural damping forces,

$$\mathscr{D}_{\mathrm{flu}} = p_0 \frac{\beta}{\bar{h}_0^3}\int_0^1 \left(\frac{\partial h_0}{\partial\tau}\right)^2 \mathrm{d}y \tag{69}$$

is the rate of work done by fluid damping forces, and

$$\mathscr{P}_{nc} = 3\beta p_0 \frac{\bar{q}_y^2}{\bar{h}_0^4}\int_0^1 \frac{\partial h_0}{\partial\tau}\frac{\partial h_0}{\partial y}\,\mathrm{d}y \tag{70}$$

is the rate of work done by nonconservative fluid friction forces.

For analysis of (64) we will follow Benjamin's approach, as given in his discussion of the energy balance in articulated fluid-conveying pipes (Benjamin, 1961, p. 468).

The net energy delivered to the rod by the flowing fluid during one period of oscillation, $T = 2\pi/\omega$, is given by

$$\Delta\mathscr{W} = -\int_0^{\mathrm{T}} (\mathscr{D}_{\mathrm{str}} + \mathscr{D}_{\mathrm{flu}} + \mathscr{P}_{nc})\,\mathrm{d}\tau. \tag{71}$$

For *harmonic* vibrations the net change in total mechanical energy $[\mathscr{T} + \mathscr{V}_i + \mathscr{V}_e]_0^T$ during one period is zero. Then, from (64), $\Delta\mathscr{W}$ must also be zero. The damping power terms $\mathscr{D}_{\mathrm{str}}$ and $\mathscr{D}_{\mathrm{flu}}$ are positive definite, as seen from (68) and (69). They are also independent of the steady flow rate $\bar{q}_y$. Energy is thus constantly dissipated during vibrations, meaning that $\Delta\mathscr{W} < 0$ when $\bar{q}_y$ is zero or small.

To have $\Delta\mathscr{W} = 0$ (with $\bar{q}_y > 0$) it is necessary that

$$\int_0^{\mathrm{T}}\int_0^1 \frac{\partial h_0}{\partial\tau}\frac{\partial h_0}{\partial y}\,\mathrm{d}y\,\mathrm{d}\tau < 0. \tag{72}$$

This means that rod sections must slope backward to the direction of motion over 'most' part of the length, just as by the well-known cantilevered fluid conveying pipe (Benjamin, 1961; Païdoussis, 1998). When (72) is satisfied and the flow rate $\bar{q}_y$ is increased further, $\Delta\mathscr{W}$ will become larger than zero, and unstable (amplified) vibrations (flutter) will set in. Harmonic vibrations exist thus only at the verge to flutter instability.

Exactly at this point (the stability/flutter limit) the deflection h_0 can be written as

$$h_0(y,\tau) = A(y)\cos(\omega\tau + \phi(y)). \tag{73}$$

Inserting this expression into (72) and carrying out the time integration gives

$$\pi\int_0^1 A(y)^2\frac{\partial\phi}{\partial y}\mathrm{d}y < 0. \tag{74}$$

This equation shows that $\partial\phi/\partial y$ necessarily must be less than 0 at least for those values of y where $A(y)$ is large.

It is noted that the spatial gradient of ϕ is the wavenumber κ in a *travelling wave* solution on the form $h_0(y,\tau) = A(y)\cos(\omega\tau - \kappa y + \phi_0)$, ϕ_0 being a constant, that is, $\kappa = -\partial\phi/\partial y$ (Lighthill, 1978, p. 241; Whitham, 1999, p. 364).

Fig. 9 shows the phase angle $\phi(y)$ for the pinned–pinned rod in air flow. The (bending) wavenumber $\kappa(= -\partial\phi/\partial y)$ takes a positive value in the whole range $0.3 < y < 0.6$. In this domain the rod vibrates much like the said cantilevered fluid-conveying pipe. Near the ends, κ is decreasing towards zero, and the travelling wave dies out.

Returning to (71), this equation shows, together with (70), that *fluid friction*, represented by the parameter β, is *the sole mechanism behind the flutter instability*.

This implies that the instability should change from flutter to divergence if the fluid viscosity is reduced beyond a certain level. Fig. 11 verifies this. Data is the same as used in Fig. 8(a), except that the kinematic viscosity ν is multiplied by 10^{-6}. Instead of flutter at $\bar{V}_{cr} = 11.80\,\mathrm{m\,s^{-1}}$, divergence is now initiated at $\bar{V}_{cr} = 19.00\,\mathrm{m\,s^{-1}}$. With the very low kinematic viscosity, this corresponds to a critical Reynolds number $\mathrm{Re}_{cr} = 1.3\times10^9$.

The kinematic viscosity was likewise reduced in the case of Fig. 10, but here flutter continues to prevail. The cantilevered fluid conveying pipe (Païdoussis, 1998) may provide a possible explanation. Here the dynamics is independent of fluid friction (Benjamin, 1961), and the flutter instability is caused solely by the last ('centrifugal force') term in (59).

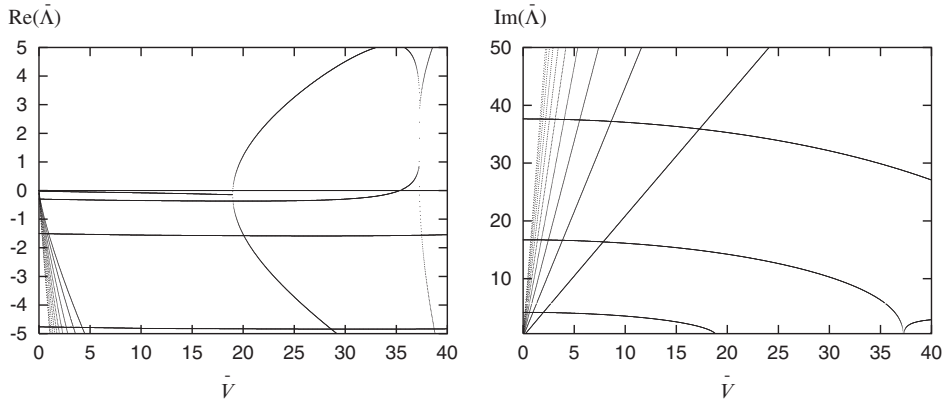

Fig. 11. The case of Fig. 8 repeated with the very small kinematic viscosity $\nu = 1.5 \times 10^{-11}\,\mathrm{m^2\,s^{-1}}$ (the actual value of air $\times\, 10^{-6}$). Divergence is initiated at $\bar{V}_{cr} = 19.00\,\mathrm{m\,s^{-1}}$ ($\mathrm{Re}_{cr} = 1.3 \times 10^9$).

That the turbulent model predicts a lower critical flow speed than the laminar model by flutter (Fig. 7) can be understood qualitatively by the fact that the random motions of turbulence increase the effective value of the kinematic viscosity ν (Lighthill, 1986, p. 75). Thus the (negative) nonconservative fluid friction force (70) is, at a given flow rate, and other things being equal, smaller (larger in terms of absolute value) by turbulent flow. [This does not apply to the *cantilevered* rod of Fig. 10, where the laminar flow model gives the lowest critical speed—again because the onset of flutter not is governed solely by viscous forces.]

That the flutter instability is characterized by a travelling (progressive) wave is in agreement with, and supports, the ideas put forward by Inada (2004) in connection with a study of a clamped–clamped elastic plate in leakage flow. Inada considers the dispersion relation to an equation analogous to (59), obtained by inserting a travelling wave solution on the form $h_0(y,\tau) = \text{constant} \times \exp[\mathrm{i}(\omega\tau - \kappa y)]$, and finds with a given ω (obtained from numerical solution of the boundary value problem) that one of the roots κ of the resulting sixth-order polynomial corresponds to a forward travelling wave. Returning to the dispersion relation, Inada finds that this root can be responsible for negative damping, which in turn is responsible for the onset of flutter. He also points out that this mechanism is different from the negative damping flutter mechanism, caused by a fluid force delay, which can occur in the related one-degree-of-freedom leakage-flow system considered as a special case in Inada and Hayama (1990). [A rigid plate allowed only translational motion, not rotational motion.]

The motion of the said one-degree-of-freedom system for onset of instability is basically a standing wave (of very simple form, though), contrary to the travelling wave in the continuous system. A referee raised the question of whether such an instability is also possible in the continuous system. The answer is that, it is not possible for the configurations considered here, as a standing wave is not a possible solution of (59) with $\bar{q}_y > 0$. This is because the terms $2(\bar{q}_y/\bar{h}_0^2)\partial^2 h_0/\partial\tau\partial y$ and $3\beta(\bar{q}_y/\bar{h}_0^4)\partial h_0/\partial y$, involving first-order spatial derivatives, couple the modes (Chen, 1981). And coupled modes (standing waves) make up travelling waves (Feynman et al., 1971). The standing wave-type instability may be possible if only the tip of a cantilevered rod is immersed in leakage flow, as suggested by the referee, but this will not be considered here.

10. Conclusions

In this paper we have bridged and extended the models of Li et al. (2002) and Fujita and Shintani (2001) to account for a flexible rod, with offset of the equilibrium position, in laminar or turbulent flow. The main findings can be summarized as follows.

(i) An energy balance analysis shows that divergence instability of a rod with at least pinned boundary conditions at both ends is due to centrifugal forces only; it is independent of fluid friction. This supports, and partly explains, the numerical results that inclusion of (correct) turbulent fluid friction at high Reynolds numbers (where a laminar friction model is invalid) only affects the predicted divergence speeds slightly.

(ii) The energy balance analysis also explains how a flutter instability is materialized for pinned–pinned and clamped–clamped rods. It is found that a progressive (forward/downstream travelling) wave is necessary for flutter instability. In other words, the flutter instability is characterized by a progressive wave. Also, it is explicitly shown that fluid friction is the sole mechanism behind the flutter instability.

(iii) While divergence instability is found to be quite insensitive to a 'wrong' fluid friction model, employing a laminar fluid friction model at high Reynolds numbers predicts too high critical flow speeds in cases of flutter instability of a pinned–pinned rod. Based again on the energy balance analysis, it is suggested, as a possible explanation, that this is because the instability-responsible friction force is increased, as turbulence increases the effective value of the kinematic viscosity.

Acknowledgement

We wish to thank Dr Fumio Inada of CRIEPI, Tokyo, for a helpful and inspiring discussion. We would also like to acknowledge the comments from an anonymous referee, which greatly helped to make this a better paper. The work has been supported by Mitsubishi Heavy Industries Ltd, Takasago, Japan.

Appendix A. Derivation of the friction terms in (1) and (2)

Let the flow, of velocity Υ, be in a direction characterized by the angle ψ, such that $U = \Upsilon \sin\psi$ is the circumferential velocity, and $V = \Upsilon \cos\psi$ the axial velocity.

Diffusion of momentum is governed by the term $v\partial^2\Upsilon/\partial Z^2$, where v is the kinematic viscosity, and Z is the radial coordinate, with $Z = 0$ on the rod surface and $Z = H$ on the surface of the outer rigid cylinder. Integration of this term over the gap gives

$$v\int_0^H \frac{\partial^2\Upsilon}{\partial Z^2}\,\mathrm{d}Z = v\left(\left.\frac{\partial\Upsilon}{\partial Z}\right|_{Z=H} - \left.\frac{\partial\Upsilon}{\partial Z}\right|_{Z=0}\right). \tag{A.1}$$

For fully developed *laminar flow* between two plates,[5] the velocity profile takes the hyperbolic form (Fox and McDonald, 1985, p. 336)

$$\Upsilon = 6\frac{Q}{H}\left\{\frac{Z}{H} - \frac{Z^2}{H^2}\right\}, \tag{A.2}$$

where Q is the flow rate, see Eq. (4). Inserting (A.2) into (A.1), the right-hand side of (A.1) can be written as

$$-12v\frac{Q}{H^3}. \tag{A.3}$$

For fully developed *turbulent flow*, the velocity gradient very close to the walls is assumed to be constant (Fox and McDonald, 1985, p. 353),

$$\left.\frac{\partial\Upsilon}{\partial Z}\right|_{Z=0} = \Upsilon_*^2/v, \quad \left.\frac{\partial\Upsilon}{\partial Z}\right|_{Z=H} = -\Upsilon_*^2/v. \tag{A.4}$$

Here Υ_* is the so-called friction velocity, defined as

$$\Upsilon_* = \sqrt{\sigma/\rho}, \quad \sigma = \frac{\lambda}{4}\frac{\rho}{2}\frac{Q^2}{H^2}, \tag{A.5}$$

where σ is the wall shear stress, ρ is the fluid density, and

$$Q^2 = H\int_0^H \Upsilon^2\,\mathrm{d}Z. \tag{A.6}$$

[5]See the explanation of the 'small-gap' approximation given in Section 2.

When (A.4) and (A.5) are inserted into (A.1), the right-hand side of (A.1) can be written as

$$-\frac{\lambda}{4}\frac{Q^2}{H^3}. \tag{A.7}$$

Appendix B. Details concerning linearization of the friction terms

Inserting (9) into the X and Y components of the squared flow rates (5) and keeping only constant terms and terms linear in the disturbances, the flow rate components reduce as follows:

$$\begin{aligned}(Q^2)_X = QQ_X &= \{\Delta Q_X^2 + (\bar{Q}_Y + \Delta Q_Y)^2\}^{1/2}\Delta Q_X \\ &= \bar{Q}_Y\left(1 + 2\frac{\Delta Q_Y}{\bar{Q}_Y} + \frac{\Delta Q_X^2}{\bar{Q}_Y^2} + \frac{\Delta Q_Y^2}{\bar{Q}_Y^2}\right)^{1/2}\Delta Q_X \\ &= \bar{Q}_Y\left(1 + \frac{\Delta Q_Y}{\bar{Q}_Y} + \mathcal{O}\left(\frac{\Delta Q_X^2}{\bar{Q}_Y^2}\right) + \mathcal{O}\left(\frac{\Delta Q_Y^2}{\bar{Q}_Y^2}\right)\right)\Delta Q_X \\ &\approx \bar{Q}_Y\Delta Q_X,\end{aligned} \tag{B.1}$$

$$\begin{aligned}(Q^2)_Y = QQ_Y &= \{\Delta Q_X^2 + (\bar{Q}_Y + \Delta Q_Y)^2\}^{1/2}(\bar{Q}_Y + \Delta Q_Y) \\ &= \bar{Q}_Y\left(1 + \frac{\Delta Q_Y}{\bar{Q}_Y} + \mathcal{O}\left(\frac{\Delta Q_X^2}{\bar{Q}_Y^2}\right) + \mathcal{O}\left(\frac{\Delta Q_Y^2}{\bar{Q}_Y^2}\right)\right)(\bar{Q}_Y + \Delta Q_Y) \\ &\approx \bar{Q}_Y^2 + 2\bar{Q}_Y\Delta Q_Y.\end{aligned} \tag{B.2}$$

Next (B.1) and (B.2) are inserted in the friction terms $\frac{1}{4}\lambda(Q^2)_X/H^3$ and $\frac{1}{4}\lambda(Q^2)_Y/H^3$. Keeping only unsteady terms, and only terms up to first order in the disturbances, the friction terms are reduced as follows:

Laminar case:

$$\begin{aligned}\frac{\lambda}{4}\frac{(Q^2)_X}{H^3} &= \frac{1}{4}\frac{48}{\bar{Q}_Y/\nu}\left(1 - \frac{\Delta Q_Y}{\bar{Q}_Y}\right)\left(\frac{1}{\bar{H}^3} - \frac{3}{\bar{H}^4}\Delta H\right)\bar{Q}_Y\Delta Q_X \\ &\approx 12\nu\frac{\Delta Q_X}{\bar{H}^3},\end{aligned} \tag{B.3}$$

$$\begin{aligned}\frac{\lambda}{4}\frac{(Q^2)_Y}{H^3} &= \frac{1}{4}\frac{48}{\bar{Q}_Y/\nu}\left(1 - \frac{\Delta Q_Y}{\bar{Q}_Y}\right)\left(\frac{1}{\bar{H}^3} - \frac{3}{\bar{H}^4}\Delta H\right)(\bar{Q}_Y^2 + 2\bar{Q}_Y\Delta Q_Y) \\ &\approx 12\nu\frac{\Delta Q_Y}{\bar{H}^3} - 36\nu\frac{\bar{Q}_Y}{\bar{H}^4}\Delta H,\end{aligned} \tag{B.4}$$

which agree with the corresponding terms in Eqs. (6) and (7) of Fujita and Shintani (2001).

Turbulent case:

$$\begin{aligned}\frac{\lambda}{4}\frac{(Q^2)_X}{H^3} &= \frac{1}{4}0.26\left(\frac{\bar{Q}_Y}{\nu}\right)^{-0.24}\left(1 - 0.24\frac{\Delta Q_Y}{\bar{Q}_Y}\right)\left(\frac{1}{\bar{H}^3} - \frac{3}{\bar{H}^4}\Delta H\right)\bar{Q}_Y\Delta Q_X \\ &\approx \frac{1}{4}0.26\left(\frac{\bar{Q}_Y}{\nu}\right)^{-0.24}\frac{\bar{Q}_Y}{\bar{H}^3}\Delta Q_X,\end{aligned} \tag{B.5}$$

$$\begin{aligned}\frac{\lambda}{4}\frac{(Q^2)_Y}{H^3} &= \frac{1}{4}0.26\left(\frac{\bar{Q}_Y}{\nu}\right)^{-0.24}\left(1 - 0.24\frac{\Delta Q_Y}{\bar{Q}_Y}\right)\left(\frac{1}{\bar{H}^3} - \frac{3}{\bar{H}^4}\Delta H\right)(\bar{Q}_Y^2 + 2\bar{Q}_Y\Delta Q_Y) \\ &\approx \frac{1}{4}0.26\left(\frac{\bar{Q}_Y}{\nu}\right)^{-0.24}\left\{1.76\frac{\bar{Q}_Y}{\bar{H}^3}\Delta Q_Y - 3\frac{\bar{Q}_Y^2}{\bar{H}^4}\Delta H\right\}.\end{aligned} \tag{B.6}$$

By making use of the definitions (12) and (18), the two sets of expressions, (B.3)–(B.4) and (B.5)–(B.6), can be unified as given in (15) and (16).

Appendix C. Offset correction functions

Including terms up to $\mathcal{O}(e^3)$ in the Taylor expansions of $\bar{h}^{-1}, \bar{h}^{-2}, \ldots$, the functions $\varepsilon_1, \varepsilon_2, \ldots, \varepsilon_9$, appearing in (45)–(47), are given by

$$\begin{aligned}
&\varepsilon_1 = 1 + \frac{1}{2}\frac{e^2}{\bar{h}_0 r_0} + \frac{1}{4}\frac{e^2}{\bar{h}_0^2} - \frac{3}{8}\frac{e^4}{\bar{h}_0^3 r_0}, \quad \varepsilon_2 = 1 + \frac{e^2}{\bar{h}_0 r_0} + \frac{3}{4}\frac{e^2}{\bar{h}_0^2} - \frac{3}{2}\frac{e^4}{\bar{h}_0^3 r_0},\\
&\varepsilon_3 = 1 + \frac{3}{2}\frac{e^2}{\bar{h}_0 r_0} + \frac{3}{2}\frac{e^2}{\bar{h}_0^2} - \frac{15}{4}\frac{e^4}{\bar{h}_0^3 r_0}, \quad \varepsilon_4 = 1 + \frac{5}{4}\frac{e^2}{\bar{h}_0 r_0} + \frac{3}{2}\frac{e^2}{\bar{h}_0^2} - \frac{3}{4}\frac{e^4}{\bar{h}_0^3 r_0},\\
&\varepsilon_5 = 1 + \frac{7}{4}\frac{e^2}{\bar{h}_0 r_0} + 3\frac{e^2}{\bar{h}_0^2} + \frac{3}{4}\frac{e^4}{\bar{h}_0^3 r_0}, \quad \varepsilon_6 = 1 + \frac{3}{4}\frac{e^2}{\bar{h}_0 r_0} + \frac{3}{4}\frac{e^2}{\bar{h}_0^2},\\
&\varepsilon_7 = 1 + \frac{9}{4}\frac{e^2}{\bar{h}_0 r_0} + \frac{9}{2}\frac{e^2}{\bar{h}_0^2}, \quad \varepsilon_8 = 1 + 3\frac{e^2}{\bar{h}_0 r_0} + \frac{15}{2}\frac{e^2}{\bar{h}_0^2},\\
&\varepsilon_9 = 1 + \frac{3}{2}\frac{e^2}{\bar{h}_0 r_0} + \frac{9}{4}\frac{e^2}{\bar{h}_0^2}.
\end{aligned} \tag{C.1}$$

Appendix D. Implementation of fluid boundary conditions

The fluid boundary conditions (47) are included in the left-hand side of the y-momentum equation (46), in its Galerkin weak form, via integration by parts, as follows:

$$\begin{aligned}
\ell_e \int_0^1 \mathbf{N}^{\mathrm{T}} \frac{\partial f}{\partial y}\,\mathrm{d}\zeta &= \int_0^1 \mathbf{N}^{\mathrm{T}} \frac{\partial f}{\partial \zeta}\,\mathrm{d}\zeta = [\mathbf{N}^{\mathrm{T}} f]_{\zeta=1} - [\mathbf{N}^{\mathrm{T}} f]_{\zeta=0} - \int_0^1 \frac{\partial \mathbf{N}^{\mathrm{T}}}{\partial \zeta} f\,\mathrm{d}\zeta\\
&= \frac{p_0}{\varepsilon^2}\,\xi_{\mathrm{ex}}\,\frac{\varepsilon_9}{\bar{h}_0^2}\,\bar{q}_y \left[\mathbf{N}^{\mathrm{T}}\left(q_{y0} - \frac{\bar{q}_y}{\bar{h}_0} h_0\right)\right]_{\zeta=1} + \frac{p_0}{\varepsilon^2}(1+\xi_{\mathrm{in}})\frac{\varepsilon_9}{\bar{h}_0^2}\,\bar{q}_y \left[\mathbf{N}^{\mathrm{T}}\left(q_{y0} - \frac{\bar{q}_y}{\bar{h}_0} h_0\right)\right]_{\zeta=0}\\
&\quad - \int_0^1 \frac{\partial \mathbf{N}^{\mathrm{T}}}{\partial \zeta} f\,\mathrm{d}\zeta,
\end{aligned} \tag{D.1}$$

where $\ell_e = L/N_e$ is the element length.

Appendix E. Element matrices

The element matrices appearing in (50) are given by

$$\begin{aligned}
&[\mathbf{M}_f]_e = \varepsilon_1 \frac{p_0}{\bar{h}_0}\,\mathbf{A}_1, \quad [\mathbf{C}_{fh1}]_e = \varepsilon_2 \frac{p_0}{\bar{h}_0^2}\,\bar{q}_y \mathbf{A}_2 + \varepsilon_3 \alpha \bar{q}_y \frac{p_0}{\bar{h}_0^3}\,\mathbf{A}_1,\\
&[\mathbf{C}_{fq1}]_e = \varepsilon_1 \frac{p_0}{\bar{h}_0}\,\mathbf{A}_2, \quad [\mathbf{S}_{fq1}]_e = \varepsilon_3 \alpha \bar{q}_y \frac{p_0}{\bar{h}_0^3}\,\mathbf{A}_2 + \varepsilon_2 \frac{p_0}{\bar{h}_0^2}\,\bar{q}_y \mathbf{A}_3, \quad [\mathbf{F}_{f1}]_e = \mathbf{A}_2.
\end{aligned} \tag{E.1}$$

Those appearing in (51) are given by

$$\begin{aligned}
&[\mathbf{C}_{fh2}]_e = \varepsilon_4 \frac{p_0}{\bar{h}_0^2}\,\bar{q}_y \mathbf{A}_1, \quad [\mathbf{C}_{fq2}]_e = -\varepsilon_6 \frac{p_0}{\bar{h}_0}\,\mathbf{A}_1,\\
&[\mathbf{S}_{fh2}]_e = \varepsilon_7 \frac{p_0}{\bar{h}_0^3}\,\bar{q}_y^2 \mathbf{A}_2 + 3\alpha\varepsilon_8 \frac{p_0}{\bar{h}_0^4}\,\bar{q}_y^2 \mathbf{A}_1 + \varepsilon_9 \frac{p_0}{\bar{h}_0^3}\,\bar{q}_y^2 \{\xi_{\mathrm{ex}} \delta_{eN_e} \mathbf{A}_5 + (1+\xi_{\mathrm{in}})\delta_{e1}\mathbf{A}_6\},\\
&[\mathbf{S}_{fq2}]_e = -\varepsilon_5 \frac{p_0}{\bar{h}_0^2}\,\bar{q}_y \mathbf{A}_2 - (1+\Xi)\alpha\varepsilon_7 \frac{p_0}{\bar{h}_0^3}\,\bar{q}_y \mathbf{A}_1 - \varepsilon_9 \frac{p_0}{\bar{h}_0^2}\,\bar{q}_y \{\xi_{\mathrm{ex}} \delta_{eN_e} \mathbf{A}_5 + (1+\xi_{\mathrm{in}})\delta_{e1}\mathbf{A}_6\},\\
&[\mathbf{F}_{f12}]_e = \varepsilon^2 \mathbf{A}_4,
\end{aligned} \tag{E.2}$$

where δ_{ij} is the Kronecker delta. Finally, those appearing in (52) are given by

$$[\mathbf{M}_s]_e = m\mathbf{A}_1, \quad [\mathbf{C}_s]_e = c\mathbf{A}_7, \quad [\mathbf{K}_s]_e = k\mathbf{A}_7, \quad [\mathbf{F}_s]_e = \mathbf{A}_1. \tag{E.3}$$

The element matrices $\mathbf{A}_1, \mathbf{A}_2, \ldots, \mathbf{A}_7$ are

$$\mathbf{A}_1 = \zeta_e \int_0^1 \mathbf{N}^{\mathrm{T}}\mathbf{N}\,\mathrm{d}\zeta, \quad \mathbf{A}_2 = \int_0^1 \mathbf{N}^{\mathrm{T}}\frac{\partial \mathbf{N}}{\partial \zeta}\,\mathrm{d}\zeta, \quad \mathbf{A}_3 = \frac{1}{\zeta_e}\int_0^1 \mathbf{N}^{\mathrm{T}}\frac{\partial^2 \mathbf{N}}{\partial \zeta^2}\,\mathrm{d}\zeta,$$
$$\mathbf{A}_4 = \int_0^1 \frac{\partial \mathbf{N}^{\mathrm{T}}}{\partial \zeta}\mathbf{N}\,\mathrm{d}\zeta, \quad \mathbf{A}_5 = [\mathbf{N}^{\mathrm{T}}\mathbf{N}]_{\zeta=1}, \quad \mathbf{A}_6 = [\mathbf{N}^{\mathrm{T}}\mathbf{N}]_{\zeta=0},$$
$$\mathbf{A}_7 = \frac{1}{\zeta_e^3}\int_0^1 \frac{\partial^2 \mathbf{N}^{\mathrm{T}}}{\partial \zeta^2}\frac{\partial^2 \mathbf{N}}{\partial \zeta^2}\,\mathrm{d}\zeta \tag{E.4}$$

Using the shape function vector (Cook et al., 1989)

$$\mathbf{N} = \{1 - 3\zeta^2 + 2\zeta^3 \quad (\zeta - 2\zeta^2 + \zeta^3)\ell_e \quad 3\zeta^2 - 2\zeta^3 \quad (-\zeta^2 + \zeta^3)\ell_e\} \tag{E.5}$$

(with $0 \leqslant \zeta \leqslant 1$), these matrices are evaluated as

$$\mathbf{A}_1 = \frac{\zeta_e}{420}\begin{bmatrix} 156 & 22\ell_e & 54 & -13\ell_e \\ & 4\ell_e^2 & 13\ell_e & -3\ell_e^2 \\ & & 156 & -22\ell_e \\ \text{symm.} & & & 4\ell_e^2 \end{bmatrix}, \quad \mathbf{A}_2 = \frac{1}{60}\begin{bmatrix} -30 & 6\ell_e & 30 & -6\ell_e \\ -6\ell_e & 0 & 6\ell_e & -\ell_e^2 \\ -30 & -6\ell_e & 30 & 6\ell_e \\ 6\ell_e & \ell_e^2 & -6\ell_e & 0 \end{bmatrix},$$
$$\mathbf{A}_3 = \frac{1}{30\zeta_e}\begin{bmatrix} -36 & -33\ell_e & 36 & -3\ell_e \\ -3\ell_e & -4\ell_e^2 & 3\ell_e & \ell_e^2 \\ 36 & 3\ell_e & -36 & 33\ell_e \\ -3\ell_e & \ell_e^2 & 3\ell_e & -4\ell_e^2 \end{bmatrix}, \quad \mathbf{A}_4 = \frac{1}{60}\begin{bmatrix} -30 & -6\ell_e & -30 & 6\ell_e \\ 6\ell_e & 0 & -6\ell_e & \ell_e^2 \\ 30 & 6\ell_e & 30 & -6\ell_e \\ -6\ell_e & -\ell_e^2 & 6\ell_e & 0 \end{bmatrix},$$
$$\mathbf{A}_5 = \zeta_e\begin{bmatrix} 0 & 0 & 0 & 0 \\ & 0 & 0 & 0 \\ & & 1 & 0 \\ \text{symm.} & & & 0 \end{bmatrix}, \quad \mathbf{A}_6 = \zeta_e\begin{bmatrix} 1 & 0 & 0 & 0 \\ & 0 & 0 & 0 \\ & & 0 & 0 \\ \text{symm.} & & & 0 \end{bmatrix},$$
$$\mathbf{A}_7 = \frac{1}{\zeta_e^3}\begin{bmatrix} 12 & 6\ell_e & -12 & 6\ell_e \\ & 4\ell_e^2 & -6\ell_e & 2\ell_e^2 \\ & & 12 & -6\ell_e \\ \text{symm.} & & & 4\ell_e^2 \end{bmatrix}, \tag{E.6}$$

where $\zeta_e = \ell_e/L = 1/N_e$.

References

Barbone, P.E., Crighton, D.G., 1994. Vibrational modes of submerged elastic bodies. Applied Acoustics 43, 295–317.

Benjamin, T.B., 1961. Dynamics of a system of articulated pipes conveying fluid. I. Theory. Proceedings of the Royal Society of London A 261, 457–486.

Bishop, R.E.D., Fawzy, I., 1976. Free and forced oscillations of a vertical tube containing a flowing fluid. Philosophical Transactions of the Royal Society of London 284, 1–47.

Chen, S.-S., 1981. Fluid damping for circular cylindrical structures. Nuclear Engineering and Design 63, 81–100.

Chen, S.-S., Rosenberg, G.S., 1975. Dynamics of a coupled shell-fluid system. Nuclear Engineering and Design 32, 302–310.

Cook, R.D., Malcus, D.S., Plesha, M.E., 1989. Concepts and Applications of Finite Element Analysis. Wiley, New York.

Feynman, R.P., Leighton, R.B., Sands, M., 1971. The Feynman Lectures on Physics, vol. 1. Addison-Wesley, Reading, MA.

Fox, R.W., McDonald, A.T., 1985. Introduction to Fluid Mechanics. Wiley, New York.

Fujita, K., Shintani, A., 2001. Axial leakage flow-induced vibration of the elastic rod as the axisymmetric continuous flexible beam. Journal of Pressure Vessel Technology 123, 421–428.

Fujita, K., Morikazu, H., Shintani, A., 2004. Dynamic behavior of pre- and post-instability of an axisymmetric elastic beam subjected to axial leakage flow. In: de Langre, E., Axisa, F. (Eds.), Flow-Induced Vibration 2004, vol. I, pp. 57–62.

Hawthorne, W.R., 1961. The early development of the dracone flexible barge. Proceedings of the Institution of Mechanical Engineers 175, 52–83.

Herrmann, G., 1971. Dynamics and stability of mechanical systems with follower forces. NASA CR-1782, National Aeronautics and Space Administration, Washington, DC.

Hirs, G.G., 1973. A bulk flow theory for turbulence in lubricant films. Journal of Lubrication Theory 95, 137–146.

Inada, F., 1999. A study on leakage-flow-induced vibration of a continuous system (consideration of a self-excited oscillation mechanism of a beam mode using wave theory). In: Flow-Induced Vibration—1999 (ASME), PVP-vol. 389, pp. 177–184.

Inada, F., 2004. Mechanism of leakage-flow-induced vibrations of continuous system. In: de Langre, E., Axisa, F. (Eds.), Flow-Induced Vibration 2004, vol. I, pp. 215–220.

Inada, F., Hayama, S., 1990. A study on leakage-flow-induced vibrations. Part 1: fluid-dynamic forces and moments acting on the walls of a narrow tapered passage. Journal of Fluids and Structures 4, 395–412.

Inada, F., Hayama, S., 2000. Mechanism of leakage-flow-induced vibrations—single-degree-of-freedom and continuous systems. In: Ziada, S., Staubli, T. (Eds.), Flow-Induced Vibration 2000, pp. 837–844.

Kaneko, S., Tanaka, S., Watanabe, T., 2000. Leakage flow induced flutter of highly flexible structures. In: Ziada, S., Staubli, T. (Eds.), Flow-Induced Vibration 2000, pp. 837–844.

Langthjem, M., 1994. On the influence of damping in a problem of dynamic stability optimization. Structural Optimization 7, 227–236.

Langthjem, M.A., Sugiyama, Y., 2000. Dynamic stability of columns subjected to follower loads: a survey. Journal of Sound and Vibration 238, 809–851.

Lesoinne, M., Sarkis, M., Hetmaniuk, U., Farhat, C., 2001. A linearized method for the frequency analysis of three-dimensional fluid/structure interaction problems in all flow regimes. Computer Methods in Applied Mechanics and Engineering 190, 3121–3146.

Li, D.-W., Kaneko, S., Hayama, S., 2002. A study on annular leakage-flow-induced vibrations. Journal of Fluids and Structures 16, 909–930.

Lighthill, J., 1978. Waves in Fluids. Cambridge University Press, Cambridge.

Lighthill, J., 1986. An Informal Introduction to Theoretical Fluid Dynamics. Oxford University Press, Oxford.

Mulcahy, T.M., 1980. Fluid forces on rods vibrating in finite length annular regions. Shock and Vibration Digest 15, 11–15.

Païdoussis, M.P., 1966. Dynamics of flexible slender cylinders in axial flow. Part 1. Theory. Journal of Fluid Mechanics 26, 717–736.

Païdoussis, M.P., 1973. Dynamics of cylindrical structures subjected to axial flow. Journal of Sound and Vibration 29, 365–385.

Païdoussis, M.P., 1996. Fluid-structure interactions between axial flows and slender structures. In: Tatsumi, T., Watanabe, E., Kambe, T. (Eds.), Theoretical and Applied Mechanics 1996. Elsevier Science B.V., Amsterdam, pp. 427–442.

Païdoussis, M.P., 1998. Fluid-Structure Interactions. Slender Structures and Axial Flow, vol. 1. Academic Press, San Diego.

Païdoussis, M.P., 2004. Fluid-Structure Interactions. Slender Structures and Axial Flow, vol. 2. Elsevier Academic Press, Amsterdam.

Païdoussis, M.P., Pettigrew, M.J., 1979. Dynamics of flexible cylinders in axisymmetrically confined axial flow. Journal of Applied Mechanics 46, 37–44.

Païdoussis, M.P., Mateescu, D., Sim, W.-G., 1990. Dynamics and stability of a flexible cylinder in a narrow coaxial cylindrical duct, subjected to annular flow. Journal of Applied Mechanics 57, 232–240.

Press, W.H., Teukolsky, S.A., Vetterling, W.T., Flannery, B.P., 1992. Numerical Recipes in Fortran. The Art of Scientific Programming, second ed. Cambridge University Press, Cambridge.

Schlichting, H., 1968. Boundary-Layer Theory, sixth ed. McGraw-Hill, New York.

Shimoyama, Y., Yamada, Y., 1957. Experiments on the labyrinth packing (1st report). Transactions of Japan Society of Mechanical Engineers, Part 3 23, 44–49 (in Japanese).

Sugimoto, N., 1996. Aeroelastic stability of a beam travelling in a tunnel lined with resonators. American Institute of Aeronautics and Astronautics Journal 34, 2005–2013.

Sugiyama, Y., Tanaka, Y., Kishi, T., Kawagoe, H., 1985. Effect of a spring support on the stability of pipes conveying fluid. Journal of Sound and Vibration 100, 257–270.

Tanaka, S., Hirata, T., Kaneko, S., Watanabe, T., 2001. Aerodynamic vibrations of combined rigid bodies due to leakage-flow. In: Pettigrew, M.J. (Ed.), Proceedings of the ASME Pressure Vessels and Piping Conference, Atlanta, GA. Flow-Induced Vibration: Axial Flow, Piping Systems, Other Topics-Volume 2, pp. 45–52.

Weaver, D.S., Ziada, S., Au-Yang, M.K., Chen, S.S., Païdoussis, M.P., Pettigrew, M.J., 2000. Flow-induced vibrations in power and process plant components—progress and prospects. Journal of Pressure Vessel Technology 122, 339–348.

Whitham, G.B., 1999. Linear and Nonlinear Waves. Wiley, New York.

Wu, X., Kaneko, S., 2005. Linear and nonlinear analyses of sheet flutter induced by leakage flow. Journal of Fluids and Structures 20, 927–948.

Zienkiewicz, O.C., Taylor, R.L., 1991. The Finite Element Method, vol. 2. Solid and Fluid Mechanics—Dynamics and Non-Linearity. McGraw-Hill, London.